Brake Squeal

A study on the fundamental cause of bicycle brake squeal

Robbin Walhout
May 2019
TU Delft

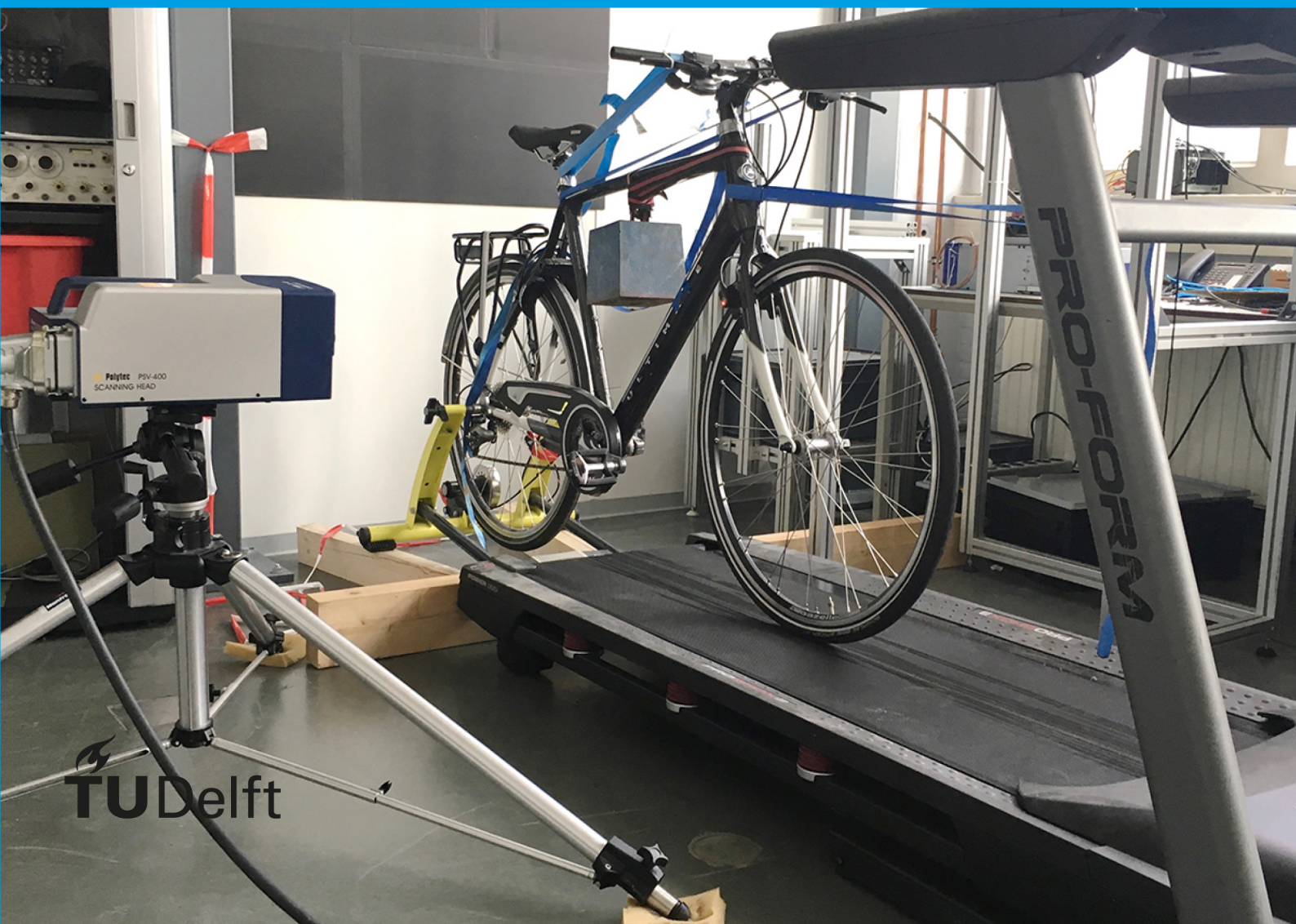

Brake squeal

A study on the fundamental cause of bicycle brake squeal

by

Robbin Walhout

Student number: 4149343
Project duration: September, 2018 – May, 2019
Supervisor: Dr. ir. A.L. Schwab

TU Delft

Preface

Since my childhood I have developed a passion for bicycles. Besides riding on my road bike, I like to restore old road bicycles from the 80's and 90's. It is an honor to me to contribute in the bicycle industry by doing this graduation project.
However, doing research is not always fun. In the first few months of my project, I struggled a lot to get my project off the ground. Doing research is a lot different than just taking classes and studying for exams. It felt like being thrown into the deep end. Luckily, after 4 months things started to fall into place.
I want to thank my supervisors Arend Schwab and Jaap Meijaard, who helped me through the process. I also want to thank Jos van Driel. He helped me a lot with setting up my experiments. Finally, I want to thank the Koninklijke Gazelle for providing bicycles and bicycle parts for this project.

Robbin Walhout
Delft, May 2019

Summary

Brake squeal is a well know problem in the bicycle industry. Most of the time brake squeal occurs due to wear of the brake components and/or in certain environmental conditions (e.g. rain and dirt). Bicycle brake squeal is often solved by trial and error. Compared to automotive industry, there is not much research done on the fundamental cause of bicycle brake squeal. As a result, bicycle brands are not able to guarantee that their bicycles will not produce squeal noise over time.
The goal of this graduation project is to get more insight into the fundamental cause of bicycle brake squeal and to find the crucial parameters that influence bicycle brake squeal.

Brake squeal is caused by friction induced vibration. Friction between the brake pads and the rim causes the brake pads and the rim to vibrate with a certain frequency. These vibrations are transmitted to other bicycle parts (e.g. front fork and spokes). In Chapter 2 these vibrations of different bicycle parts were measured by using an accelerometer and a laser vibrometer. It turned out that all measured bicycle parts were vibrating in the same squeal frequency of approximately 1100 Hz. Also, the surface scanning results of front fork showed a torsional vibration of the front fork 'legs'. After adding a brake booster the torsional vibration mode was gone. From these observations it was concluded that the torsional stiffness of the front fork legs is probably an important factor when it comes bicycle brake squeal propensity.

Chapter 3-6 talks about the parameters that might influence bicycle brake squeal. In total there are 17 potential squeal parameters. However, only 5 of them are studied in this graduation project: the bending and torsional stiffness of the front fork, the friction coefficient of the brake pads, the spoke tension and the out-of-plane stiffness of the wheel. The stiffness's of four different front forks were measured: two aluminum forks, a carbon fork and a fork made of steel. Changing the fork influences the squeal frequency and the squeal propensity of the bicycle. The results showed that a stiffer fork has a lower squeal propensity and a higher squeal frequency.
In Chapter 5 the static and dynamic friction coefficients of four different brake pads were measured. All measured brake pads showed a relative large difference between the static and dynamic friction coefficients, indicating that stick-slip is probably the fundamental cause of the bicycle brake squeal. However, the different friction coefficients of the different brake pads did not influence the squeal frequency or the squeal propensity of the bicycle.
In Chapter 6, the spoke tension was varied, to study the influence of the spoke tension and the out-of-plane stiffness of the wheel on brake squeal, since the spoke tension and the out-of-plane stiffness of the wheel are directly related. The results showed that the spoke tension doesn't influence the squeal frequency or the squeal propensity. The same conclusion can be drawn for the out-of-plane stiffness of the wheel.
In conclusion, bicycle brake squeal is most likely caused by stick-slip behavior of the brake pads on the rim. Also, the properties of the front fork seem to be the most crucial parameters when it comes to bicycle brake squeal. However, only 5 of the 17 parameter were studied in this graduation project. This means that this project is only a starting point into the world of bicycle brake squeal.

From the experiments it was concluded that the stiffness and the mass of the front fork determines whether a bicycle is going to squeal. A big advantage of the front fork stiffness is that it doesn't change over time. Other parameters like friction coefficient of the brake pads, spoke tension and weather conditions are changing over time. To solve the problem, the front fork has to be designed such that brake squeal can never occur, independently of all the other parameters. Therefore, it is recommended to focus on the fork further research on bicycle brake squeal.

Contents

1 Introduction **1**
- 1.1 Background information . . . 1
- 1.2 Literature study (a summery) . . . 1
  - 1.2.1 Friction . . . 1
  - 1.2.2 Friction induced vibration. . . . 2
  - 1.2.3 Brake squeal . . . 6
  - 1.2.4 Experimental studies on bicycle brake squeal . . . 7
  - 1.2.5 Bicycle brake squeal models. . . . 10
  - 1.2.6 Conclusion of literature study . . . 17
- 1.3 Research problem . . . 18
- 1.4 First experiments . . . 18
- 1.5 Report structure . . . 18

2 First measurements **19**
- 2.1 Measurements with accelerometer . . . 19
  - 2.1.1 Experimental setup . . . 19
  - 2.1.2 Results . . . 21
  - 2.1.3 Conclusion . . . 24
- 2.2 Measurements with laser doppler vibrometer . . . 25
  - 2.2.1 How a laser doppler vibrometer works . . . 25
  - 2.2.2 Experimental setup . . . 26
  - 2.2.3 Experimental setup . . . 27
  - 2.2.4 Single point measurements . . . 27
  - 2.2.5 Surface measurements . . . 29
- 2.3 Discussion and Conclusion . . . 32

3 Potential squeal parameters **33**

4 Front fork stiffness **35**
- 4.1 Measuring bending stiffness . . . 36
- 4.2 Measuring torsional stiffness. . . . 39
  - 4.2.1 Measuring the squeal frequencies of the front forks . . . 42
- 4.3 Discussion and Conclusion . . . 44

5 Friction coefficient **45**
- 5.1 Experimental setup . . . 45
- 5.2 Measuring the static coefficient of friction . . . 47
- 5.3 Measuring the dynamic coefficient of friction . . . 49
- 5.4 Discussion and Conclusion . . . 53

6 Spoke tension **55**
- 6.1 Experimental setup . . . 55
- 6.2 Working principle of a spoke tension meter and calibration . . . 55
- 6.3 Measurement procedure . . . 56
- 6.4 Results . . . 56
- 6.5 Discussion and Conclusion . . . 57

7 Discussion **59**

8 Conclusion **61**

9 Recommendations **63**

A **65**

B **67**

C **69**

Bibliography **71**

1

Introduction

Bicycle brake squeal is a well know problem in the bicycle industry. Most of the time brake squeal occurs due to wear of the brake components and/or in certain environmental conditions (rain and dirt). Bicycle brake squeal is often solved by trial and error. Well known solutions are cleaning the rim and brake pads or replacing the brake pads.

1.1. Background information

This research assignment has its origin at the bicycle manufacturer Koninklijke Gazelle. This bicycle brand experiences an increase in bicycle brake squeal since the use of Magura hydraulic brakes. Apparently Magura hydraulic brakes have a higher squeal propensity. Different methods were tried to solve this problem: cleaning the rim and brake pads, changing the rim, the tire and front fork of the bicycle. Sometimes the squeal was gone, but for other bicycles the problem kept existing. Adding a double Magura booster was found to be the most effective method. Still, there isn't found a solution that rules out squealing for all bicycles in all possible environmental conditions.

1.2. Literature study (a summery)

It is commonly known that brake squeal is caused by friction induced vibration. In order to understand brake squeal on a more fundamental level, it is important to understand the underlying fundamental mechanisms of squeal.

1.2.1. Friction

In general friction can be defined as the resistance to motion when two surfaces slide against each other [18]. In case of braking, friction is a useful phenomenon, because it is an effective method to slow down a vehicle. On the other hand, there are also unwanted side-effects of friction, for example heat generation, wear and brake squeal. In order to prevent these unwanted side effects, it is needed to understand the friction on a more fundamental level.
On microscopical level, dry sliding contact friction can be described as elastic and plastic deformations of asperities in contact, where each asperity caries a part f_i of the normal load F_N (figure 5.4).

Due to the normal load F_N the asperities will deform until the total contact area of all asperities is large enough to carry the load. The contact area of each asperity contact point is $a_i = f_i/H$, where H is the hardness of the material. When the hardness of the materials of the two bodies is different, the softest hardness has to be used in the formula. The total contact area can be written as $A_r = F_N/H$. For a small normal load the deformation of the asperities is elastic. When the normal load increases the deformation of the asperities becomes plastic when the shear pressure exceeds the shear strength τ_y of the softest surface material. In sliding, the friction force can be described as $F_T = \tau_y A_R$ and the friction coefficient $\mu = F_T/F_N = \tau_y/H$ [26].

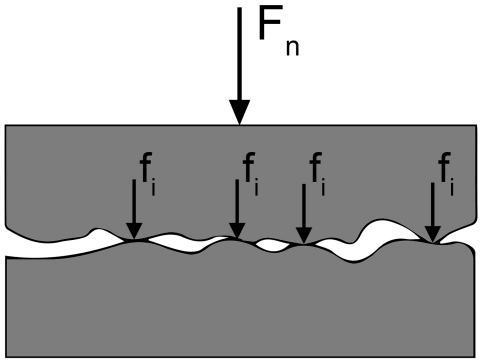

Figure 1.1: Friction on microscopic scale

1.2.2. Friction induced vibration

Friction induced vibration is a typical self-excited vibration phenomenon and a major concern in a wide variety of mechanical applications, such as automobile friction belts, vehicle brake systems, precision machine tools and mechanical gear systems. Commonly friction induced vibration is considered as the unstable vibration caused by contact forces between two interfaces sliding against each other. Especially with dry contact sliding, friction can cause a variety of instabilities such as stick-slip, quasiharmonic oscillation, chatter, squeal, mode-coupling and sprag-slip [27],[9].
Friction induced vibration is a very complex phenomenon and is sensitive to a variety of variables, such as properties of both materials, surface texture, usage history, sliding speed, normal load and environmental conditions. Depending on the normal load four different friction regions can be distinguished. This division of friction regions is based on a pin-on-disc sliding experiment (figure 1.2). The four friction regions are [7]:

1. Linear region; in which the friction force increases linear with the normal load with a constant friction coefficient.
2. Non-linear region, where the friction coefficient is no longer constant, but increases when the normal load increases.
3. In the transient region the friction force varies in a intermittent way.
4. The last region is the self-excited vibration region where friction force causes high amplitude periodic self excited vibrations.

This complexity makes it hard to model friction induced vibration. In history there are several attempts made to model this phenomenon. According to Keitzel and Hoffmann, there are four theories describing friction induced vibration: stick-slip-limit-cycle, mode coupling, sprag-slip and a variable dynamic friction coefficient [11].

The stick-slip oscillator theory

As mentioned earlier stick-slip is one of the unstable friction modes caused by dry contact sliding. The oscillator stick-slip model is basically a mass-spring system moving on a rough surface, as shown in figure 1.3. The gravitational force of the mass induces a dry sliding contact force between the mass and the moving rough surface. In this model the motion of the mass can be distinguished into a stick mode, where the mass and the moving surface have the same velocity and a slip mode, in which the mass and the moving surface have different velocities. The mass and the base have the same speed until the spring force becomes bigger than the static friction force. As the mass starts to slide relatively to the surface, the motion will be ruled by the dynamic friction force (which is smaller than the static friction force). Due to this sliding motion of the mass the spring force will become smaller than the dynamic

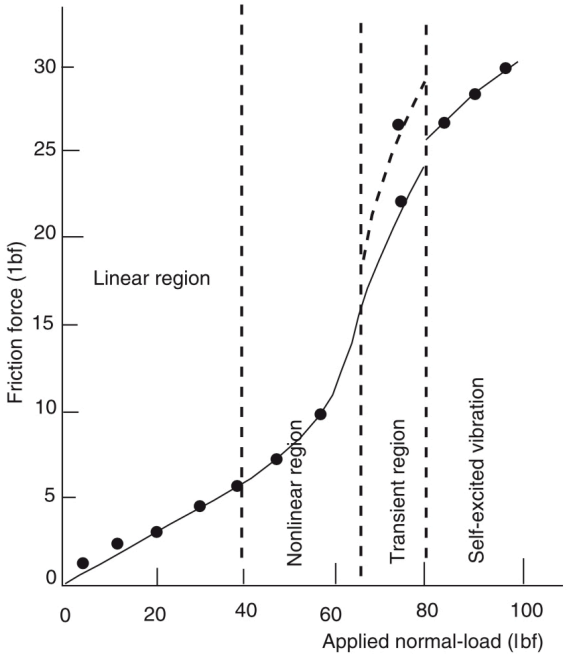

Figure 1.2: The four friction regions [9]

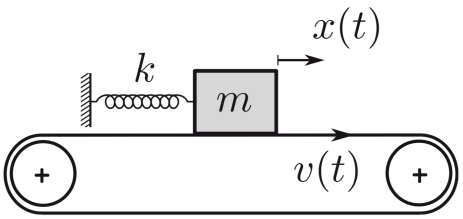

Figure 1.3: The oscillator stick-slip model consists of a mass-spring system moving on a rough surface [13]

friction force, causing the mass to stop his relative sliding to the surface. The alternation between the relative sliding and stopping is defined as the stick-slip effect. The equation of motion of the mass can be described with [13]

$$m\ddot{x}(t) + kx(t) = f(t), \tag{1.1}$$

where x is the position of the mass, k the spring stiffness, m the mass and f the frictional force. The frictional force depends on the difference between the velocity of the mass and the moving base and is defined as

$$f(t) = mg_{\mu}sgn(v(t) - \dot{x}(t)), \tag{1.2}$$

where v is the base speed and μ the friction coefficient.

Mass-spring-dashpot model

This model is an elaboration of the stick-slip model. Besides the spring it introduces a dash-pot, as shown in figure 1.4. The motion of the mass m is can be described with the following equation

$$m\ddot{x} + c\dot{x} + kx = F(v_0 - \dot{x}), \tag{1.3}$$

where c is the damping coefficient, v_0 the velocity of the moving base. The friction force F is a function of the relative velocity between the moving surface and the mass m. This function can be expressed through a Taylor series or can be experimentally determined. Two typical curves of the relation between friction force and relative velocity are shown in figure 1.5. One

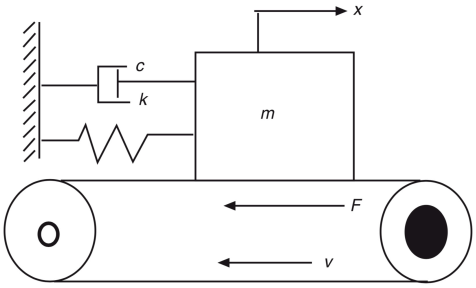

Figure 1.4: A mass-spring-dashpot system moving on a belt [9]

curve for the clockwise rotation and one curve for the counterclockwise rotation of the belt. As can be seen in figure 1.5 the friction-velocity curves have a negative slope for low values

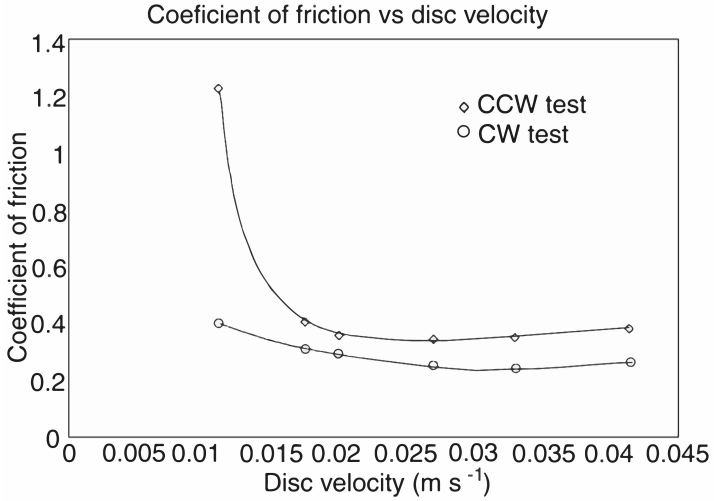

Figure 1.5: Clockwise (CW) and counterclockwise (CCW) friction-velocity curves [9]

of relative velocity. These negative slope regions can potentially lead to dynamic instability when

$$\left(2\zeta + \frac{1}{\omega_n}\frac{dF}{dv}\right) < 0 \tag{1.4}$$

From this equation it can be concluded that self-excited vibration occurs only if the viscous damping coefficient c is smaller than the slope of the friction force.

Spurr's Sprag-slip model

Where the self-exited vibration in the stick-slip model is caused by the difference between the static and dynamic friction coefficient, in the sprag-slip model the geometrical or kinematic constraints are causing unstable vibrations [5]. To describe this mechanism Spurr used a semi-rigid rod pivoted at point O (figure 1.6) and resting on a moving surface at an angle θ. The rod is pushed down at the surface with a horizontal force. When the plate moves to the left the rod will 'sprag' (or lock) due to friction between the rod and the plate. When the stress in the rod increases it will deform and will therefore release itself from the 'spragging' condition and returns in its initial position. This cycle will be repeated and could lead to sprag-slip limit cycle.
The friction force can be described with

$$F_f = \frac{\mu L}{1 - \mu tan(\theta)}, \tag{1.5}$$

where μ is the friction coefficient and L is the load. From the equation follows that the friction force F_f will approach infinity when μ approaches $cot\theta$. This explains the 'spragging' of the

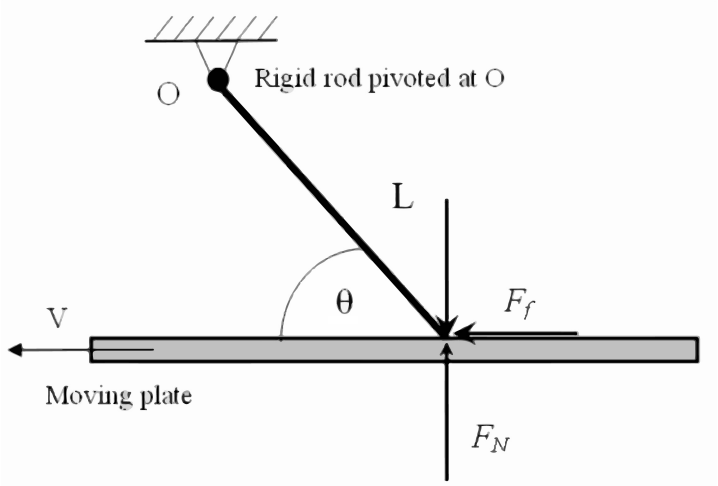

Figure 1.6: A schematic representation of the Sprag-slip model [5]

rod.

Mode Coupling

Mode coupling occurs when two surfaces vibrate in the same mode (same wavelength and frequency) creating a coupled system mode. This resonance of two components sliding against each other can induce more energy into the system than it can dissipate, resulting in squeal [5]. A schematic representation of mode coupling in brake discs is shown in figure 1.7.

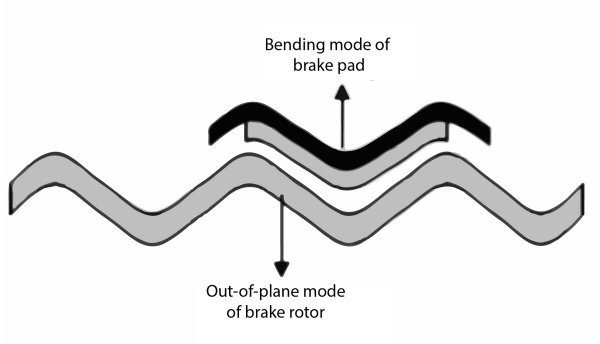

Figure 1.7: Mode coupling between two brake components [25]

Due to the mode coupling, friction damping of the components will be minimal causing the system to work as a loudspeaker, generating brake squeal [25]. Hoffmann and Gaul made a minimal model to explain the underlying physical mechanism of mode coupling. The model consists of a moving belt, a mass and three springs and is shown in figure 1.8. In this model F_f represents the Coulomb friction force and can be described by $F_f = -\mu k_3 y$ with a constant μ assumed. Furthermore, the equations of motion are [8]

$$\begin{bmatrix} m & 0 \\ 0 & m \end{bmatrix} \begin{bmatrix} \ddot{x} \\ \ddot{y} \end{bmatrix} + \begin{bmatrix} k_{11} & k_{12} - \mu k_3 \\ k_{21} & k_{22} \end{bmatrix} \begin{bmatrix} x \\ y \end{bmatrix} = \begin{bmatrix} 0 \\ 0 \end{bmatrix} \tag{1.6}$$

with

$$k_{11} = k_1 cos^2(\alpha_1) + k_2 cos^2(\alpha_2),$$

$$k_{12} = k_{21} = k_1 sin(\alpha_1) cos(\alpha_1) + k_2 sin(\alpha_2) cos(\alpha_2),$$

$$k_{22} = k_1 sin^2(\alpha_1) + k_2 sin^2(\alpha_2) + k_3.$$

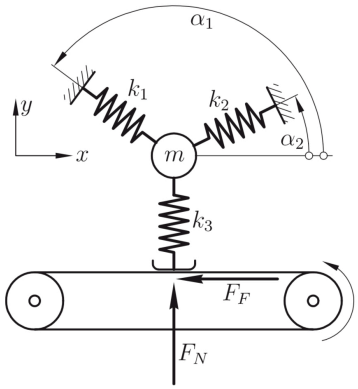

Figure 1.8: Mode coupling model by Hoffmann and Gaul [8]

1.2.3. Brake squeal

As mentioned earlier, brake squeal is caused by self-excited vibration due to friction. Some well known examples of self-excited vibration sounds are rubbing a wineglass, the squeal of sneakers on a parquet floor, chalk on a blackboard, string instruments and rail-wheel noise. On atomic scale there is kinetic energy converted to thermal energy during friction, where the kinetic energy is caused by the relative motion of the two surfaces. When there is more kinetic energy fed to the system than the system can dissipate to thermal energy, instabilities occur resulting in sound radiation [4].

Frictional noise is generally classified in two categories: rubbing noise (low frequency) and squeal noise (high frequency) [29]. Rubbing noise (or rough noise) appears when the vibration energy is small. Squeal noise occurs when the contact force is bigger and reaches beyond the interface and friction. In this case the two component friction becomes a coupled system and produces more complex and often non-linear response. This condition is called mode lock-in, because the asperities are locked in place due to the high contact force. This coupled system responds with a coupled frequency. It's dependent on the normal load, sliding velocity and contact geometry if mode lock-in occurs and it what frequency it is going to vibrate [2].

In the automotive industry a lot of research has been done on brake squeal. Brake squeal has been a problem since the introduction of the automotive vehicles. Since the brake mechanism of vehicle uses dry friction contact in combination with high friction loads, brake noise can occur easily. Brake noise with high frequency (between 1 kHz and 16 kHz), known as brake squeal, makes the driver uncomfortable [5]. Despite the fact that brake squeal has nothing to do with the brake performance of the vehicle, customers relate unwanted noise with underlying quality problems of the vehicle and therefore lose confidence in the safety of the vehicle. This makes brake squeal an expensive problem for brake and car manufacturers in terms of warranty costs. To eliminate these warranty costs a lot of research has been done on the underlying cause of disc brake squeal. There are roughly two theories for explaining the basic principle of brake squeal. The first theory is based on the fact that the coefficient of friction increases rapidly with decreasing of the vehicle speed when braking, what results in brake squeal. This theory is mainly based on the stick-slip model and was popular in the early stage of brake squeal research. Later in history, it was discovered that brake squeal occurs also with a constant friction coefficient. This led to a second theory that assumes a constant coefficient of friction and explains brake squeal with the occurring of system instabilities caused by the interaction of the structural components of the brake system. Murakami et al. proposed that brake squeal was influenced by both the μ vs speed and the structural instability factor [23]. Nowadays mode coupling is the most popular theory by most researches [17].

Figure 1.9 summarizes the different types of friction characteristics and their associated vibration types.

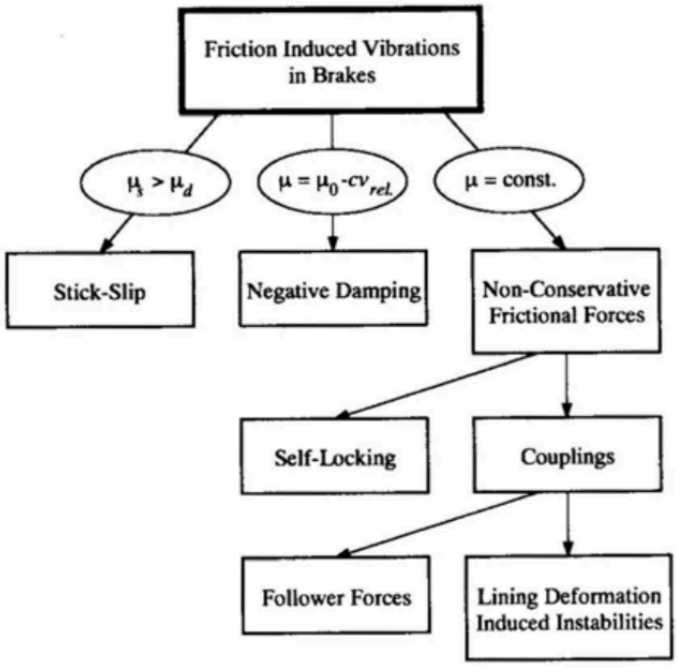

Figure 1.9: Types of friction induced vibration in brakes [6].

1.2.4. Experimental studies on bicycle brake squeal

Several experimental studies have been done on bicycle disc brake squeal. All of these studies are done on disc brakes, none of them on rim brakes. The experimental studies on bicycles that are found in literature will be discussed in this section.

Experimental study by Redfield

This study [21] was done on a disc brake of a mountain bike. The measurements were done during pedaling an braking simultaneously with the bike on a trainer and during a field test. The lateral velocity and the longitudinal acceleration of the disc brake were measured by using a laser vibrometer. The results are shown in figure 1.10. The low frequency and low amplitude velocity response is due to the weight shifting of the rider during pedaling. During braking the frequency and amplitude of the disc brake relative velocity suddenly increases until limit cycle vibration occurs and the brakes are released again. The measured dominant noise frequencies during braking were between 1200 Hz and 2100 Hz. The measured individual eigenfrequencies values of the rotor and spokes were also this frequency range. The longitudinal accelerations of the caliper were measured during the field test figure 1.10b. From this experiment it was also concluded that the brake noise in the lab setup was much more quiet compared to the field experiments. This can be explained by the lack of tire interactions with the uneven ground in the lab setup.

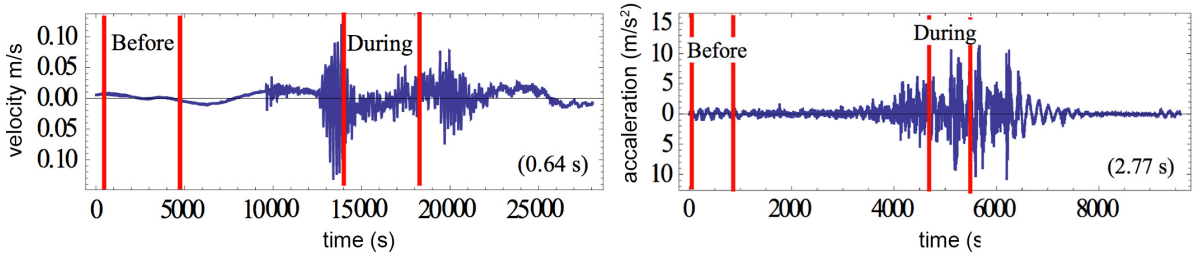

Figure 1.10: The lateral velocity (a) and the longitudinal acceleration (b) of the disc brake [21].

Experimental study by Nakae et al.

The next experimental study on bicycle disc brakes that will be discussed, is a study by Nakae et al. [15]. For the bench test an actual bicycle was used. The out-of-plane acceleration of the caliper is measured with accelerometer and a charge amplifier. The temperature of the pad was measured with a thermocouple device. The test bench setup and the in-plane and out-of-plane directions are shown in figure 1.11. In this setup the bicycle frame and back

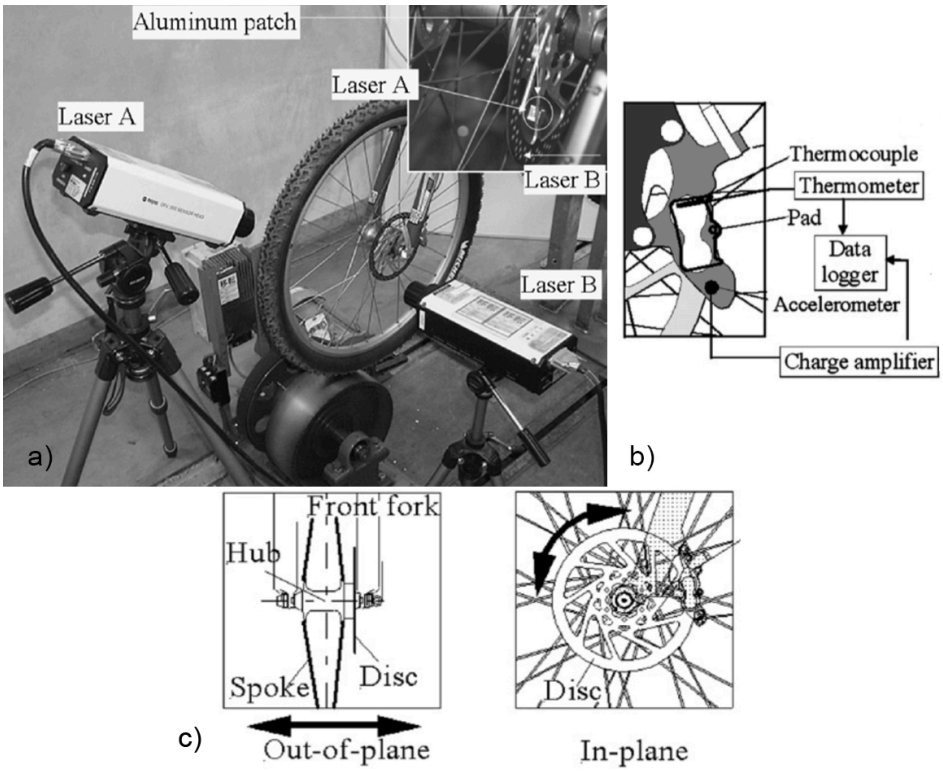

Figure 1.11: The test bench setup that is used for the experiment (a), a close up of the disc brake and sensors (b) and the in-plane and out-of-plane directions (c) [15].

wheel are fixed to the ground. The front wheel is driven by a fly wheel and can rotate freely. The in-plane and out-of-plane vibrations of the disc and spokes were measured with two laser Doppler vibrometers (figure 1.11a). A small reflective aluminum patch was mounted on the disc in order to let laser A measure the in-plane vibration. Also to the hub and a spoke a aluminum patch was attached to measure their in-plane and out-of-plane vibrations.

The microphone measured a constant squeal frequency of approximately 1 kHz. The squeal frequency was not dependent of the disc temperature or rotation speed of the wheel. Chatter, on the other hand, occurred only at temperatures above 260 ^{o}C with a constant frequency of approximately 500 Hz. However, the chatter was always generated together with the squeal and in none of the experiments did the chatter occur alone. The out-of-plane vibration modes of the disc, hub, caliper and spokes are coupled. Figure 1.12 shows the vibration modes for both squeal and chatter. Both vibration modes were fixed during the rotation of the disc. The white, gray and black squares in figure 1.12a represent the measuring points. The black area's in figure 1.12a represent the nodes of the coupled vibration.

Influence of the spokes tension to squeal

To investigate the influence of the spoke tension on squeal and chatter, the spoke tension was increased and decreases uniformly. Also, the natural frequency of each spoke was measured with a laser Doppler vibrometer by hammering the spokes in the out-of-plane direction. The results of a possible tension distribution are shown in a circular graph with radial axis coordinates (figure 1.13). The average spoke tension was approximately 900 N on the disc side and 700 N on the non-disc side. Increasing the tension of the spokes uniformly resulted in

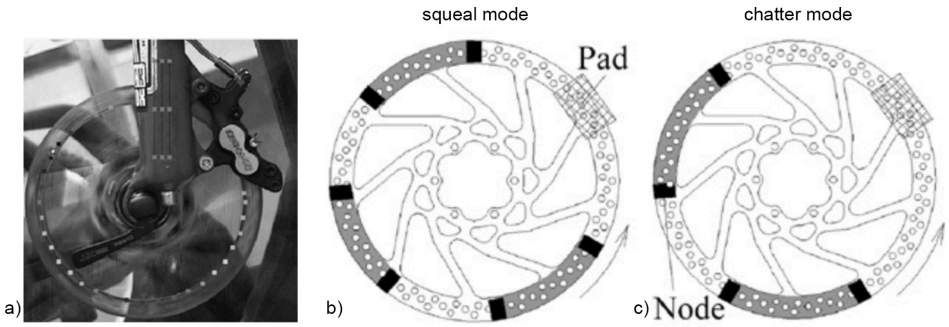

Figure 1.12: The disc, hub, caliper and spokes (a), out-of-plane vibration mode for squeal (b) and for chatter (c) [15].

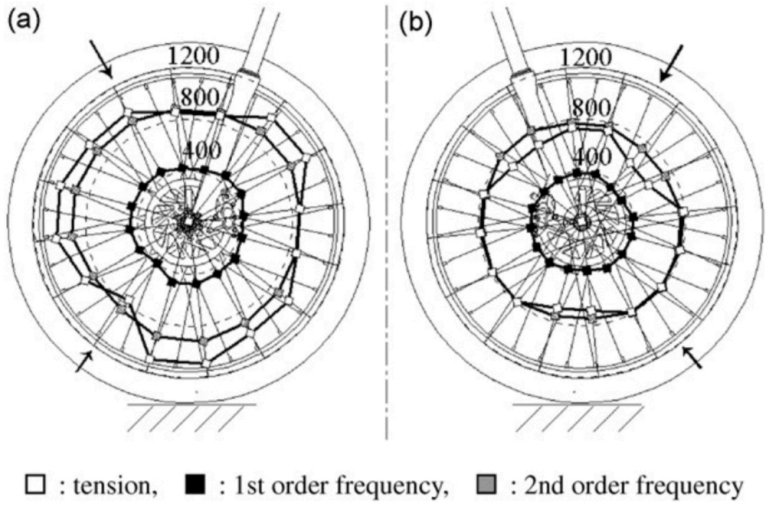

Figure 1.13: Tension [N] and natural frequency [Hz] distribution show in a circular graph of the disc side (a) and the non-disc side (b) [15].

a higher squeal frequency. And for very low spoke tension there was no squeal and chatter observed at all. To investigate the influence of the length of the spokes, a smaller wheel was used with spoke 73 mm shorter than the first test wheel. Due to the shorter spokes the squeal frequency increased from 1 kHz to 1.275 kHz. Also, chatter barely occurred with the smaller wheel setup.

Friction characteristics

In the same study another experiment was done on the characteristics of the braking friction, especially the relation between the rotational speed of the disc and the torque on the shaft during braking. The bench test setup for this experiment and the results are shown in figure 1.14. The frictional torque was measured at several constant disc speeds with a constant braking force. The results showed that the friction had a negative slope with respect to the disc velocity, what is a well known cause for brake squeal as mentioned earlier in this literature review.

Conclusion

Some important conclusions can be drawn from this study by Nakae et al.

- Bicycle disc brake squeal is caused by a coupled vibration of the combined disc, hub, caliper and spokes.
- The in-plane vibration of the disc is due to a negative slope of the friction coefficient with respect to the disc velocity.

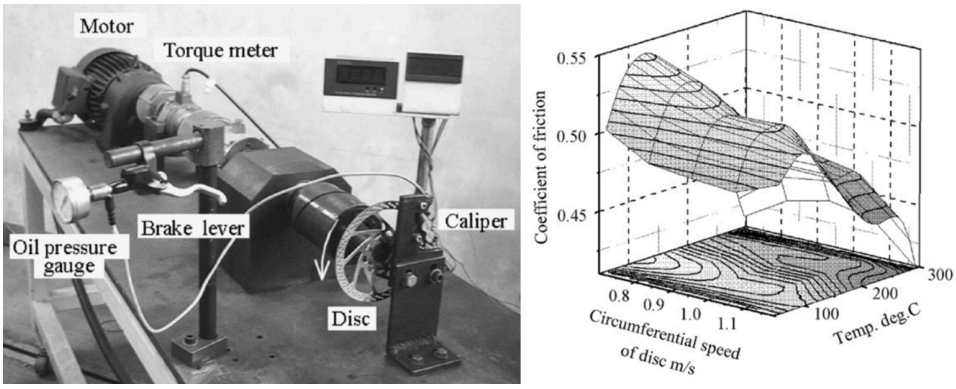

Figure 1.14: The test bench setup (a) and the results (b) [15].

- The squeal during braking has a constant frequency of around 1 kHz and is not dependent of the disc rotational speed. Chatter has a frequency of 500 Hz and occurs only at high disc temperatures.
- The tension of the spokes have an effect on the amount and the frequency of the squeal. A very low spoke tension resulted in the absence of squeal.
- The in-plane and out-of-plane of the brake components and spokes can be measured with laser Doppler vibrometers and accelerometers.

1.2.5. Bicycle brake squeal models

In literature there are only a few models found regarding the bicycle, especially mountain bike, disc brakes. Modern mountain bikes are extremely low-weight with directional designed stiffness and are equipped with high power, low-weight brakes. This leads to to high forces in the rear frame structure and brake components. According to Redfield and in contrary to the automotive disc brakes, stick-slip is believed as the main cause of vibration and noise during bicycle braking. Some of these models take besides the disc brake itself also the frame, tire and spokes into account.

Redfield model I

Redfield published two bicycle disc brake models in 2008 and in 2014. The first model is mainly focused on stability of the brake system and doesn't take other bicycle components (e.g. spokes or frame) into account. Figure 1.15 shows a schematic representation of the model.

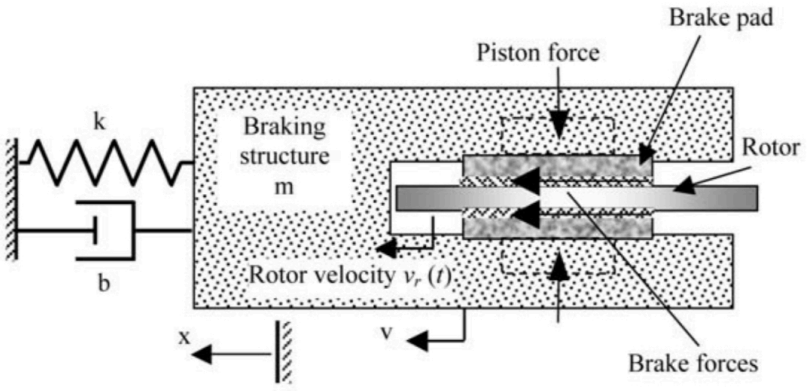

Figure 1.15: A schematic representation of the first Redfield bicycle brake model (2008) [20].

In this model the frame is considered as a solid. The stiffness k and damping b represent the deformation of the braking structure. When the rotor rotates in an anticlockwise

direction a leftwards friction force on the brake pads will be generated during braking. This friction force leads to a leftwards resultant force on the whole brake system and eventually to a vibrating motion. When the velocity of the brake structure is lower than the rotor velocity, a dynamic friction force will deform the structure. If the structure velocity reaches the rotor speed, static friction force will cause the brake pad to stick to the rotor. Due to the deformation a force will be built up in the structure until it overcomes static friction force and brake pad will slip. The stability of different friction situations will be discussed in the following sections.

Low friction force and an undamped system

As discussed earlier the friction force causes the brake system to oscillate. In the first few cases it is assumed that the brake force is applied instantaneously. When the friction force is relatively low the velocity of the brake structure will be lower than the rotor velocity, i.e. $F_k/k < v_r/\omega_n$. In this equation v_r/ω_n represents the normalized velocity of the rotor and F_k is the kinetic (or dynamic) friction force. A phase plane response of the brake system is shown in figure 1.16. The trajectory follows an orbit around the center F_k/k in a constant slip motion with a radius of $r = F_k/k$.

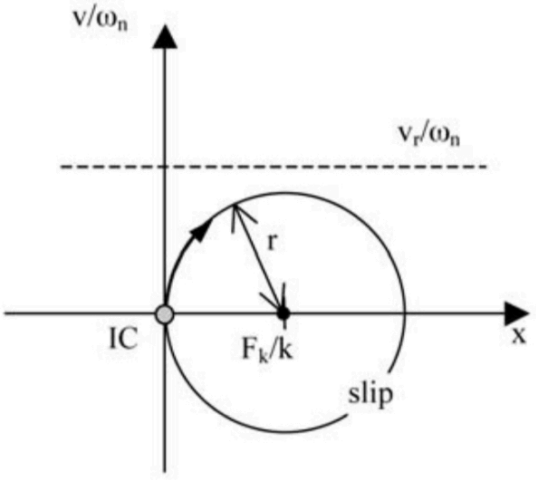

Figure 1.16: Undamped phase plane response of the brake system without sticking; $F_k/k < v_r/\omega_n$ [20].

High friction force and an undamped system

In this situation sticking will occur due to the fact that $F_k/k > v_r/\omega_n$. During sticking, the rotor and brake structure move together ($v = v_r$). The phase plane response consists of three trajectory portions as can be seen in figure 1.17. The trajectory start in the center and moves initially the same as the low force case with the same radius r_1. During the b-stick portion the structure and rotor move together until elastic deformation force overcomes the static friction force. After this, slip occurs again (c-slip) with the same orbit center as a-slip, but with a different radius:

$$r_2 = \sqrt{\left(\frac{\Delta F}{k}\right)^2 + \left(\frac{v_r}{\omega_n}\right)^2}, \qquad \Delta F = F_s - F_k. \tag{1.7}$$

As can be seen in the equation the difference between the kinetic and static friction force ΔF determines the c-slip radius, because the other variables are constant. A bigger radius will increases the chance of the occurrence of a limit-cycle stick slip. At the end of the c-slip section sticking will occur again and this stick-slip behavior will repeat itself indefinitely.

High friction force and an damped system

This situation is almost the same as the previous situation, but now with sufficient damping added to the system. The trajectory of the phase plane response starts again at the center

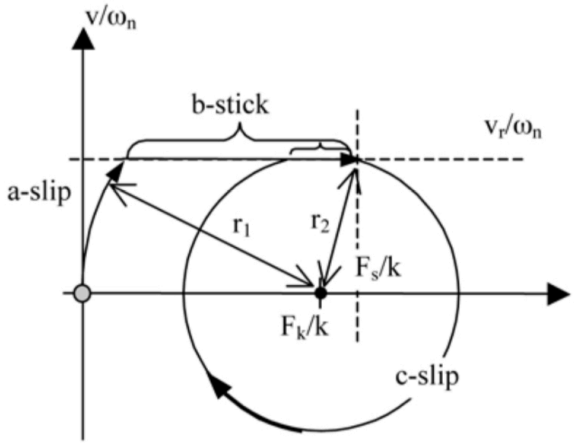

Figure 1.17: Undamped phase plane response of the brake system with sticking; $F_k/k > v_r/\omega_n$ [20].

and follows again the a-slip and b-slip sections as in figure 1.17. During the c-slip section the damping causes the trajectory to spiral into an equilibrium displacement of F_k/k as can be seen in figure 1.18. The amount of damping added to the system and the ratio $\Delta F/k$

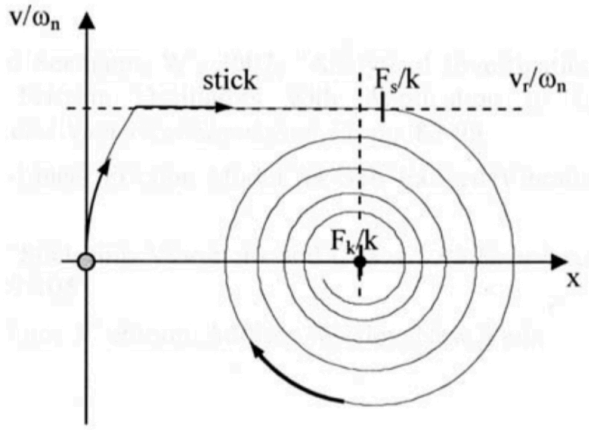

Figure 1.18: Damped phase plane response of the brake system with stick-slip; $F_k/k > v_r/\omega_n$ [20].

determines whether the system stabilizes in its equilibrium point or continues in a limit-cycle.

Non-instantaneous braking

In previous cases it was assumed that the braking force was instantaneous applied. In this last case the phase plane response of the brake system during non-instantaneous braking is analyzed. Non-instantaneous braking is assumed to be increasing exponential. The trajectory starts in the origin and moves in spiral way to its steady state center $F_k(\infty)/k$ (figure 1.19).

Conclusion

Some important conclusions can be drawn from this model.

- Adding damping to the braking system can decrease the chance of re-sticking.
- Making ΔF $(F_s - F_k)$ as small as possible by proper material selection will minimize stick-slip, especially in combination with damping.
- Non-instantaneous braking is an effective method to prevent the occurrence of stick-slip and can be achieved by adding compliance to the braking mechanism and hydraulics.

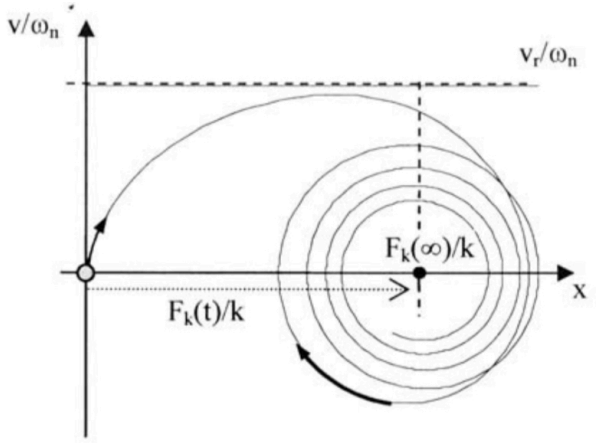

Figure 1.19: Damped phase plane response of the brake system with stick-slip; $F_k/k > v_r/\omega_n$ [20].

Redfield model II

In 2014 Redfield developed a second dynamic 2-DOF model [21]. Contrary to the first Redfield model, this model focuses mainly in on the vibration of the rear frame and the wheel. In figure 1.20a the most important forces during braking acting on the rear frame and on the wheels are shown. These forces induce the deformations of the rear frame and the rear wheel. The two most left forces apply a moment on the rear frame causes the frame to bend. The leftward force (blue) comes from the rotating wheel that is slowed down by the caliper causing a force on the mounting point of the caliper to the frame. And the frame axle force is a rightward reaction force (blue). The brake force on the rotor and the traction force on the tire cause an opposite torsion force (both black) on the wheel. These two moments causes the wheel to ”wind-up” due to the compliance of the spokes and the rim.

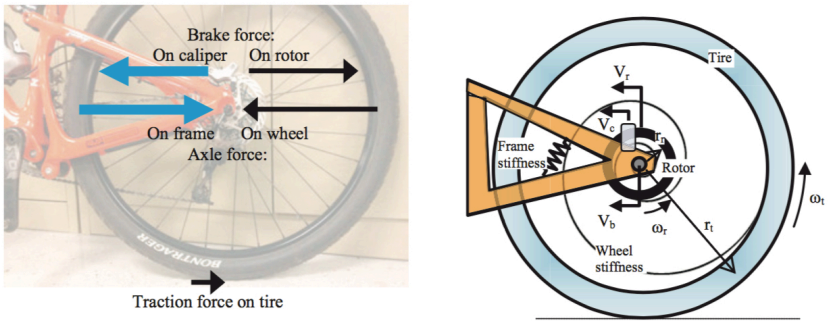

Figure 1.20: Most important braking forces (a) and a schemetic representation of the model (b) [21].

In figure 1.20b a schematic representation of the model is shown. The spring in the rear frame triangle represents the frame stiffness and the spiral line inside the wheel represents the torsional stiffness of the wheel. In this model V_r is the rotor velocity, V_c the caliper velocity, V_b the bike velocity, r_r the rotor radius, r_t the tire radius, ω_r the rotor angular velocity and ω_t the tire angular velocity.

Equations of motion

The equations of motion can be described with states variables being ω_t, V_c, θ_w and x_c, where θ_w is the torsional deflection of the wheel and x_c the deflection of the frame at the position of the caliper:

$$\dot{\omega}_r = \frac{1}{J_r}(k_t\theta_w + b_t(\omega_t - \omega_r) - r_r F_f), \qquad \dot{V}_c = \frac{1}{m_f}(F_f - k_f x_f - b_f V_c), \tag{1.8}$$

$$\dot{\theta}_w = \omega_t(t) - \omega_r, \qquad \dot{x}_c = V_c,$$

where J_r is the inertia of the tire and the rim, b_t the structural damping of the frame, m_f and k_f the mass and stiffness of the frame. k_t and b_t are the compliance and damping of the tire and spokes.

Model parameterization

The next step is to parameterize the model. The brake force is modeled as a exponential function with a first order lag to approximate the application rate of the pad force on the rotor. The average brake force and the kinetic pad-rotor friction coefficient are measured during steep downhill riding and have values of 900 N and 0.4 respectively . The application rate is dependent on development of the hand force over time and the amount of compliance of the brake components causing a delay. Frame parameters are taken from the work of Redfield and Sutela (2009). The rear frame stiffness is 350 N/mm, the translational wheel stiffness is 90 N/mm. Frequencies of the frame and wheel are respectively 300 and 200 Hz and the damping ratios of the frame and wheel are between 0.02 and 0.1. Most parameters were varied during the simulation to determine their influence on the braking performance.

Results

The results are represented with phase plane plots with on the horizontal axis the deflection normalized by the natural frequency and on the vertical axis the velocity (figure 1.21). Important parameters as frame and wheel stiffness, brake force, brake application rate and the bike velocity were varied to study their contribution to the stability of the system. In figure 1.21a shows a stable system were the rotor speed starts at approximately 0.9 m/s and the caliper speed at zero. Both velocities are relative to the bike. During braking the rotor and caliper starts to oscillate were the kinetic energy of the rotor is partly converted to the caliper causing the caliper to start moving. Over time the brake force increases what leads to a higher normalized deflection and a lower oscillation speed of both components. Finally both components reach a steady state deflection due to the steady state brake force.

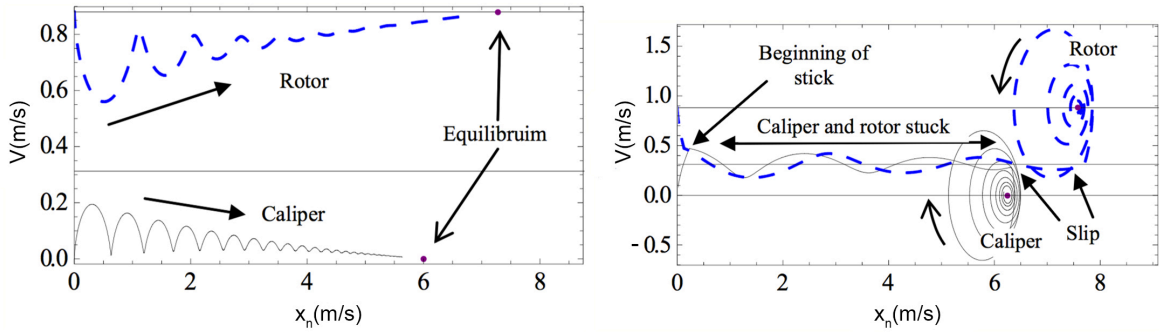

Figure 1.21: Vibration of the rotor and caliper, velocity vs. normalized deflection (a) single stiction (b) [21].

Figure 1.21b shows an example of stick-slip behavior of the system. The caliper and rotor show sticking behavior when they reach the same relative velocity causing them to stick together. Sticking can be caused by a low frame and/or wheel stiffness, a low bike velocity or a increase of brake force and/or its application rate. In figure 1.21b it can be seen that the rotor and caliper have approximately the same speed as in the stable situation. However, after a small amount of time they start moving together in a oscillating way and sticking occurs. When the braking force increases the relative deflection of both components increases causing force to build up in the system due to its compliance. When this build up force is bigger than the static friction force between the rotor and the caliper, slip occurs causing the caliper and rotor to oscillate independently until their motion is damped (figure 1.21b).

The next situation that will be discussed is re-sticking. Re-sticking can result in unstable limit-cycle behavior. Whether re-sticking occurs is mostly dependent on the damping of the system and the ratio of the static and kinetic friction. A greater μ_s/μ_k means more force

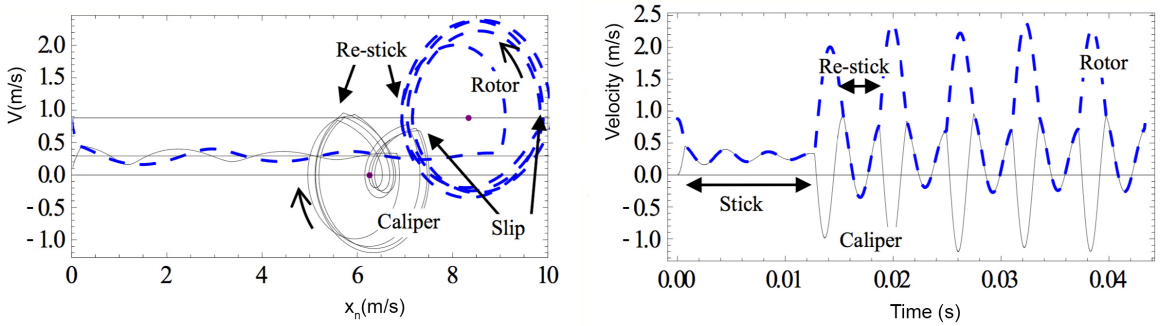

Figure 1.22: Unstable stick-slip limit cycle behavior in phase-plane (a) and time response (b) [21].

building up in the system during sticking. Also, adding damping to the system decreases the chance of re-sticking. Limit cycle behavior of the rotor and caliper is shown in figure 1.22.

The limit cycle phase plane behavior looks like the single sticking behavior (figure 1.21b). However, the difference is the oscillating orbit of the rotor and caliper stay in more or less the same orbit during limit-cycle behavior without converging to a stable equilibrium point. The time response of the limit cycle behavior shows how the rotor and caliper move together during sticking and in opposite direction during slipping. Also the frequency of the caliper is higher than the frequency of the rotor after the first time re-sticking.

Another important factor causing instability is slip sensitivity. A low slip sensitivity means a fast change from the maximum static $\mu_s N$ to dynamic friction $\mu_k N$. When the slip sensitivity is high, more negative damping is added to the system. Negative damping causes the oscillation orbit to diverge as shown in figure 1.23. The oscillation amplitude of the caliper increases until sticking occurs which ends in limit cycle behavior similar to the previous situation (figure 1.22.

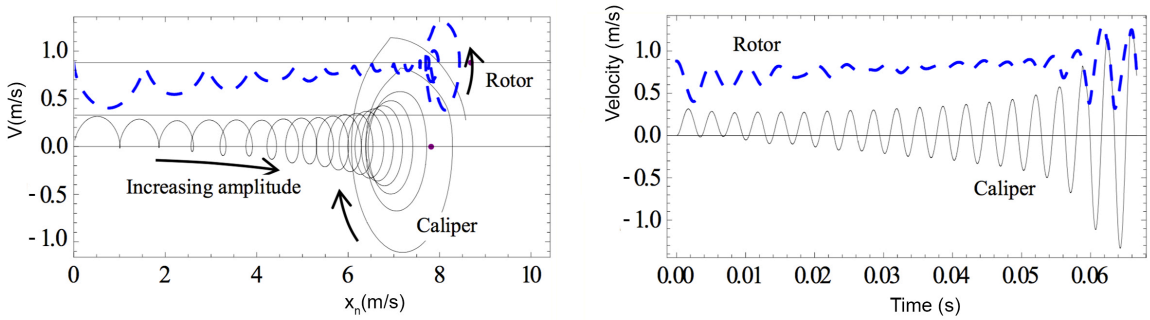

Figure 1.23: Phase plane (a) and time response (b) of the system with increased slip sensitivity [21].

Conclusion

Some important conclusions can be drawn from this second Redfield model.

- Factors that increase the propensity to vibration of components and squeal are high and quick braking, low bike velocity, low frame stiffness, low radial wheel stiffness and low system damping.
- When the static value of friction approaches the dynamic friction value slowly, more negative damping is added to the system what leads to a slowly increasing oscillation amplitude and results in limit cycle behavior.

Nakae et al. models

In 2010 the Japanese researchers Nakae, Sueoka and Ryu made two analytical models of the bicycle disc brake; a linear and a non-linear model. Both models will be discussed briefly in this section.

Linear bicycle disc brake model

This analytical model [16] consists of the disc, hub, caliper and spokes. For each component the equations of motion are defined. After that a stability analysis is done by looking at the characteristic value problem of each component. If the real part of the characteristic value is positive, unstable behavior and therefore squeal occurs. Also the imaginary part of the unstable characteristic value can be converted to a frequency. For unstable behavior, the frequency of squeal against the disc temperature is shown in figure 1.24a.

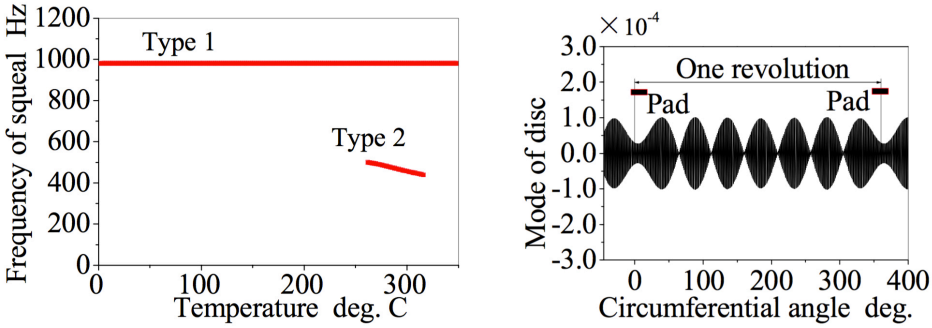

Figure 1.24: Frequency of brake noise against the temperature of the disc (a) and the out-of-plane vibration modes of the disc (b) [16].

As can be seen, two types of squeal exists. The first one (type 1) has an almost constant frequency of 980 Hz and is independent of the disc temperature, while the second one (type 2) decreases with an increasing disc temperature and has a lower frequency of approximately 490 Hz. Furthermore, in figure 1.24b the out-of-plane vibration modes of the disc are shown, where the horizontal axis represents the circumferential angle of the disc. An angle of zero degrees correspondents to the location the pad on the disc. From pad to pad is 360 degrees and is equal to one revolution. Figure 1.25 shows the in-plane vibration of the spokes on both sides of the brake disc when they are oscillating in the type 1 squeal mode. It can be clearly seen that the amplitude of the vibrating spokes is a lot bigger compared to the amplitude of the out-of-plane vibration of the disc and the amount of vibration modes is also smaller for the spokes.

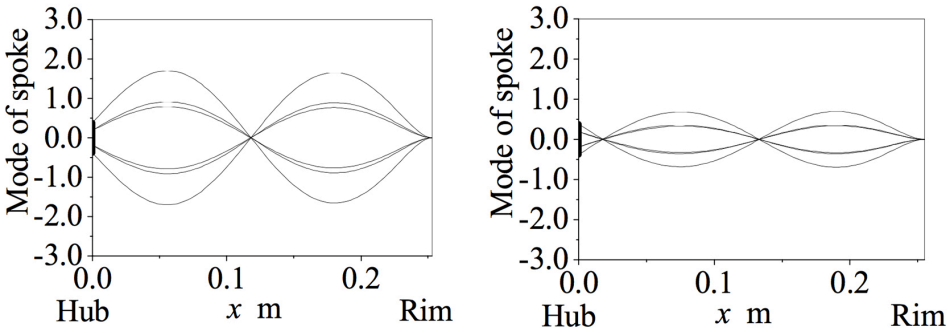

Figure 1.25: In-plane, unstable vibration of a spoke on the disc side (a) and on the other side of the disc (b) [16].

Non-linear bicycle disc brake model

The non-linear Nakae et al. model [14] takes the same bicycle components into account. Almost all equations of motion are the same as in the linear model. The main difference is that non-linear terms are included in the frictional forces acting in the disc brake system. The results of the non-linear model show also the two different types of squeal at approximately the same frequencies. However, the region where type 2 squeal occurs is smaller for the non-linear model (figure 1.26)a. Also, the amount of out-of-plane vibration modes is smaller for the non-linear model (figure 1.26)b.

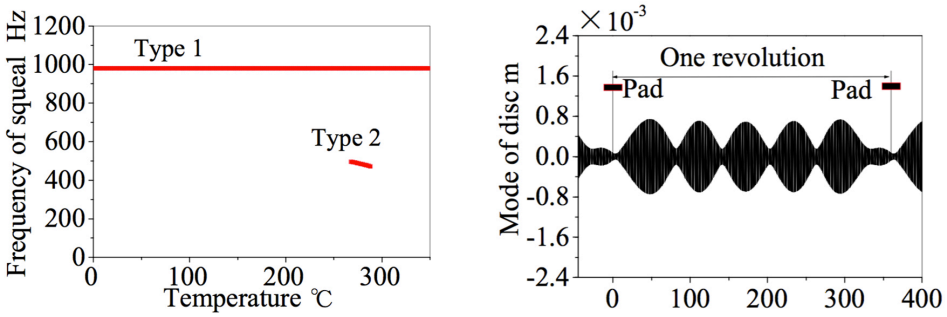

Figure 1.26: Frequency of brake noise against the temperature of the disc (a) and the out-of-plane vibration modes of the disc (b) [16].

The vibration of the spokes looks similar to the results of the linear model, except for the fact that they behave in a more chaotic way due to the non-linearity (figure 1.27).

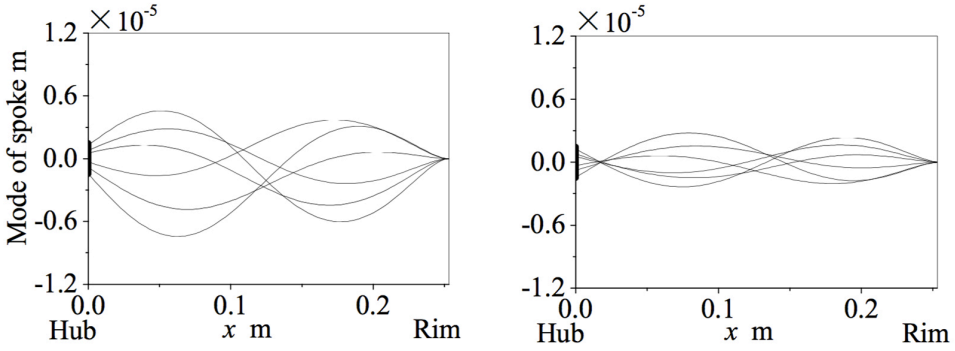

Figure 1.27: In-plane, unstable vibration of a spoke on the disc side (a) and on the other side of the disc (b) [16].

1.2.6. Conclusion of literature study

Despite decades of experimental, analytic and finite elements studies, still brake squeal remains a largely unresolved problem. However, a lot progress is made in getting insight on the factors contributing to brake squeal. Experimental studies gave a lot of information about the nature of brake squeal (e.g. vibration modes). Analytical studies showed that an unstable brake system leads to friction induced vibration and therefore to squeal. Thanks to finite element models the complex geometries of a disc brake and its boundary and loading positions can be represented more accurately. Furthermore, different material compositions, operating conditions and other brake component parameters can be changed without any costs and compared easily.
A list of relevant conclusions that can be drawn from this literature review are shown below. These conclusions form also the basis for further research on bicycle brake squeal.

- Mode coupling is believed to be the main cause of automotive brake squeal.
- In disc brakes of bicycles, both mode coupling and stick-slip are responsible for brake squeal.
- Adding damping to a bicycle braking system can decrease the chance of the occurrence of stick-slip.
- Making $\delta F(F_s - F_k)$ as small as possible by proper material selection will minimize stick-slip.
- Non-instantaneous braking is an effective method to prevent the occurrence of stick-slip and can be achieved by adding compliance to the braking mechanism and hydraulics.

- Low frame stiffness and low radial wheel stiffness increases the propensity of bicycle brake squeal.
- Bicycle disc brake squeal is often caused by a coupled vibration of the disc, hub, caliper and spokes.
- The frequency of bicycle brake squeal is not dependent on the rotational speed of the wheel.
- The tension of the spokes have an effect on the amount and the frequency of the squeal. A very low spoke tension resulted in the absence of squeal. This was the case in an experimental study on bicycle disc brakes.
- Effective methods to minimize brake squeal are applying a viscoelastic damping insulator, chamfering and/or slotting the brake pads and changing the surface roughness.

1.3. Research problem

First of all it's important to point out that the primary goal of this study is not to find a solution for brake squeal. The goal of this study is to get more insight into the fundamental cause of the problem. This brings us to the following research question:

Research question: What is the fundamental cause of bicycle brake squeal and what are the crucial parameters influencing squeal frequency and propensity?

The scope of this study is defined by the Koninklijke Gazelle: only front fork hydraulic Magura rim brakes. Other components as rim, spokes, tire and front fork can be changed. The Gazelle Ultimate in it's original configuration will be used as a starting point of this research assignment. At Gazelle, this bicycle is known for its high squeal propensity. The original configuration of this bicycle exists of a carbon front fork, Magura HS11 brakes, Gazelle VR19 alloy 6063 T6 rims and Schwalbe Spicer tires.

1.4. First experiments

In order to get to know which variables are important when it comes to brake squeal, some small experiments were performed. For these experiments the rear axis of the bicycle is fixed in a bicycle stand. The front wheel is driven by a treadmill. Different rims, brake pads, front forks and tires were tested. Also the speed of the treadmill, the air pressure in the tire and the brake force are varied. Some first conclusions can be drawn:

- Changing the rim, brake pads and tires changes only the squeal propensity, but not its frequency.
- Changing the front fork changes both the squeal propensity and the frequency.
- Increasing the speed of the treadmill doesn't change much, but decreases slightly the squeal propensity. In the future the experiments will be done at low speed (max 4 km/u). This speed is enough to let the bicycle squeal and is also safer than doing the experiments with a high treadmill speed.
- Changing the pressure tire doesn't change anything.
- Increasing the brake force increases also the loudness of the noise.

The conclusions of these first small experiments form the basis of the rest of this project.

1.5. Report structure

This report consists roughly of two parts. The first part is meant to get more insight into the fundamental cause of bicycle brake squeal (chapter 2). The second part consists of a series of experiments studying the influence of some relevant factors that probably influence bicycle brake squeal (chapter 3-6).

2

First measurements

These first measurements are meant get to more insights into the problem. As discussed earlier, brake squeal is caused by friction induced vibration. It's important to investigate which bicycle part exactly are vibrating and in which directions. Most likely, the rim and the brake pads are vibrating, because they represent the friction interfaces. However, it is also possible that other parts as the fork and the spokes are vibrating as well. Another important aspect of this experiment is to compare the vibrating frequencies of the components with the audio squeal frequency, recorded with a microphone. This will give insight into the question which bicycle parts contribute to the squeal noise.

First, some single point measurements will be done with an accelerometer and with a laser vibrometer. After that the front fork will be scanned by the laser vibrometer from the side and from the front and the rim will be scanned from the side. This will result in 3D animations of the vibration modes of the front fork and the rim.

2.1. Measurements with accelerometer

The advantage of an accelerometer is that it is small, cheap and lightweight. This makes it easy to connect the accelerometer to different bicycle parts.

2.1.1. Experimental setup

The setup for this experiment is shown in figure 2.1. The bicycle front wheel is driven by a treadmill at low speed. Using the treadmill at 2-4 km/h was enough to perform the measurements and to get decent results. Performing the measurements at low speed is also safer. Besides, there is less noise form the treadmill at low speed. Increasing the speed didn't affect the squeal frequency. However, at high speed (15-20 km/h) it became harder to let the bike squeal. Furthermore, the brake is operated by a person sitting on the saddle of the bicycle.

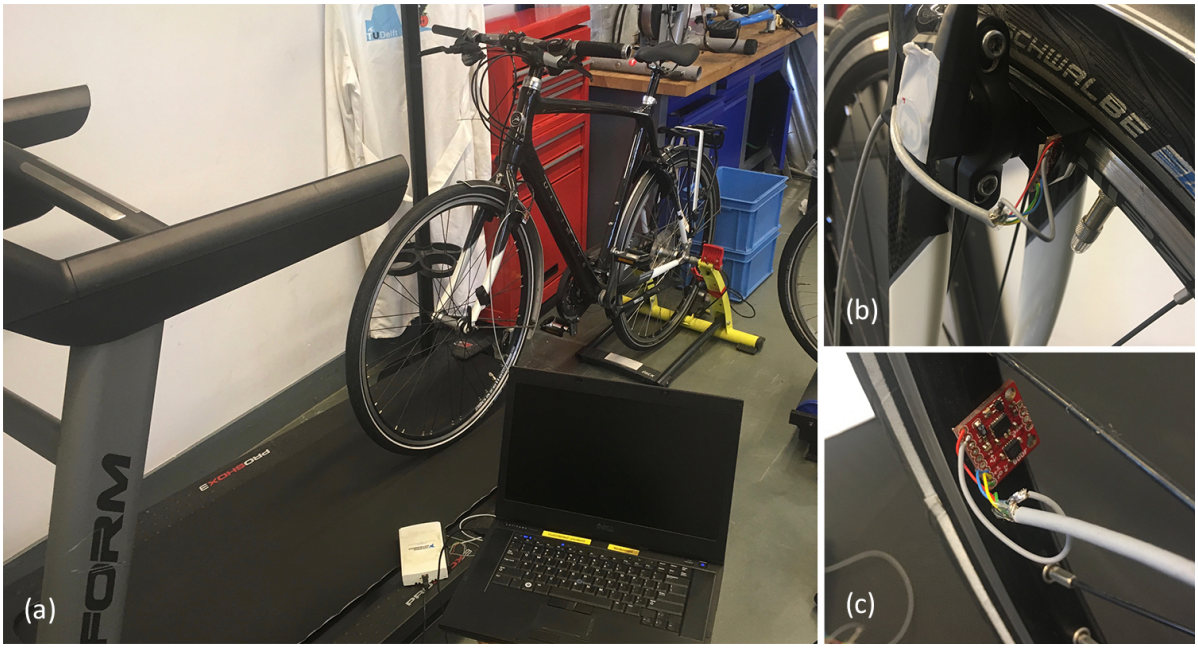

Figure 2.1: Experimental setup for measurements with an accelerometer (a), the accelerometer connected to one of the brake pad (b) and connected to the rim (c).

The bicycle that is used is a Gazelle Ultimate carbon bike. At Gazelle, this bicycle is known for its high squeal propensity. This bike in its original configuration is also the starting point for this research assignment. The bike is equipped with a carbon front fork, Magura HS11 brakes, Gazelle VR19 alloy 6063 T6 rims and Schwalbe Spicer tires.

The accelerometer that is used for this experiment is a capacitive accelerometer known as ADXL335. This sensor was connected to the bicycle parts with strong double-sided tape and at the top of the accelerometer an extra layer of tape if possible. The vibrations of the following parts were measured using an accelerometer: brake pad (figure 2.1b), rim (figure 2.1c), brake system, front fork and spokes.

The analog signal of the accelerometer is send to a Multifunction I/O device (NI USB-2612). The I/O device stores 5000 measuring points before sending it to the laptop. This way it is possible to make measurements with high measuring frequency. This amplifier box is connected to a laptop. Labview is used to store the data into a csv file. In order to measure the high frequency vibrations and to recognize the sinus shape, the measuring frequency has to be approximately 20 times larger than the squeal frequency. The squeal frequencies of this bicycle are around 1 KHz. This means that the measuring frequency has to be 20 KHz. With this measuring frequency there are approximately 20 measuring points per vibration, which will give a smooth sinus shape.

How capacitive accelerometers work

Figure 2.2 shows the basic working principle of a capacitive accelerometer. When the gray box starts moving, the mass inside the box will not follow immediately due to the inertia force working on the mass. After the acceleration the spring will cause the mass to return to its original position. The relative motion of the mass with respect to the box will change the distance between the plates and therefore the capacitance of the capacitor. The change in capacitance correspondents to the amount of acceleration. This principle applies for the x-, y- and z-direction [28]. The output signal of the accelerometer is in volt. With calibration the exact relation between the output signal and the corresponding acceleration can be determined. However, for this experiment we only need to measure the vibration frequency of the motion. Therefore, there is no need to calibrate the accelerometer.

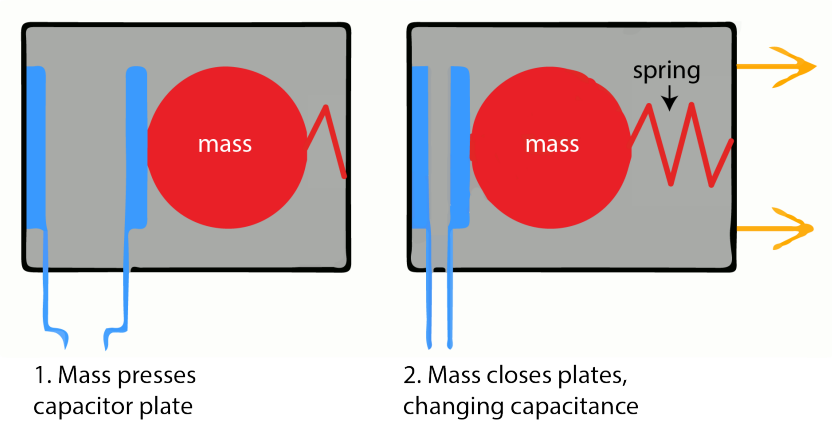

Figure 2.2: A schematic representation of the basic principle of an accelerometer [28].

2.1.2. Results

The output files has three columns, for each acceleration direction a separate column. The acceleration data in x-, y- and z-direction is stored in the first, second and third column respectively. Matlab is used to analyze the data. In order to get the frequency of each measurement, a Fast Fourier Transform (FFT) analysis is done on each dataset using Matlab. The Matlab code used of this experiment can be found in Appendix A.

Figure 5.2 shows a small portion of the raw data of the accelerometer attached to the brake system. The x-, y- and z-direction are defined in the right part of the figure. Each bicycle parts has his own local coordinate systems, because for each bicycle part the accelerometer is mounted in a different way.
In the x- and z-direction there is a very clear sinus shaped vibration signal visible without any noise. However, in the y-direction there isn't a clear signal. Also, the amplitude in y-direction is smaller compared to the amplitude in x- and z-direction. This make sense, because the rim doesn't move in the y-direction. Note that this amplitude is an acceleration amplitude in volt and not a displacement amplitude. However, a larger acceleration amplitude with the same frequency means also a larger displacement amplitude.

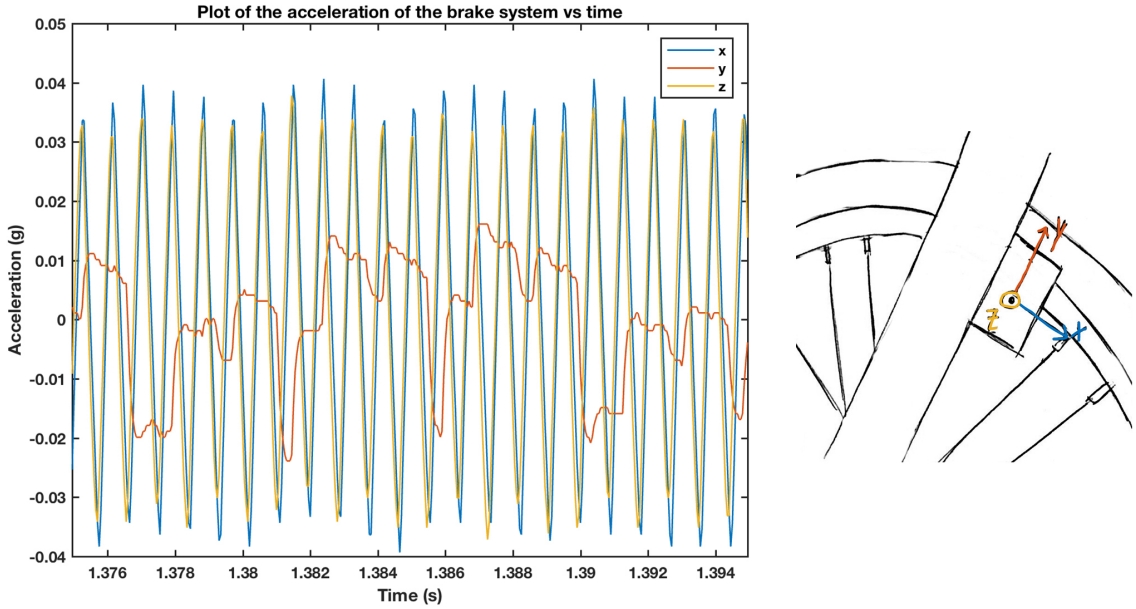

Figure 2.3: Results of the accelerometer attached to the brake system.

From the FFT analysis of the date in Matlab it appeared that the vibrating frequencies of the brake system in each direction are:
f_x = 1122 Hz f_y = - f_z = 1116 Hz.

The vibrating frequency in y-direction is left empty, because there was no clear signal visible on the graph. The measured audio frequency form microphone data is 1140 Hz. An iPhone was used as a microphone and Adobe Audition was used to extract the frequency from the mp3 file.

Figure 2.4 shows the raw data of the accelerometer attached to one of the brake pads.

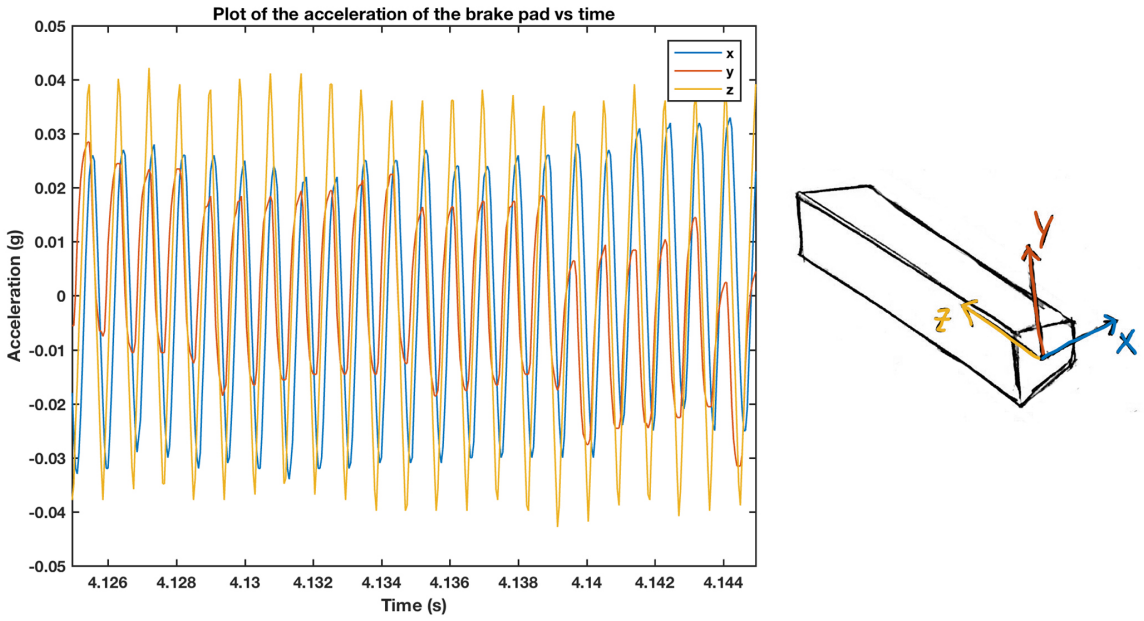

Figure 2.4: Results of the accelerometer attached to the brake pad.

In contrast to the brake system, the brake pad vibrates in all directions with a nice sinus shaped signal. This is probably due to the fact that the brake pad is not mounted rigidly to the brake system. With Magura brakes, there is always a little amount of play between the pads and the brake system. However, there is a clear difference in amplitude between the vibrations in the different directions. The amplitude in z-direction is almost twice as big as the amplitude in y-direction. This applies also to other small samples of the data and can be easily explained by the fact that the friction takes place in the z-direction. The relative large amplitude in z-direction is possibly due to the stick-slip effect between the brake pad and the rim.

The FFT analysis showed that the vibrating frequencies of the brake pad in each direction are:
f_x = 1122 Hz f_y = 1132 Hz f_z = 1127 Hz.

Next, the accelerometer is mounted to the bottom of the front fork. The results are shown in figure 2.5. It was unexpected that there is barely any movement in x-direction, while this direction is the less stiff direction of the fork. The vibrations in the y- and z-direction are probably due to resonance of the fork. In this case the front fork functions as a resonance box.

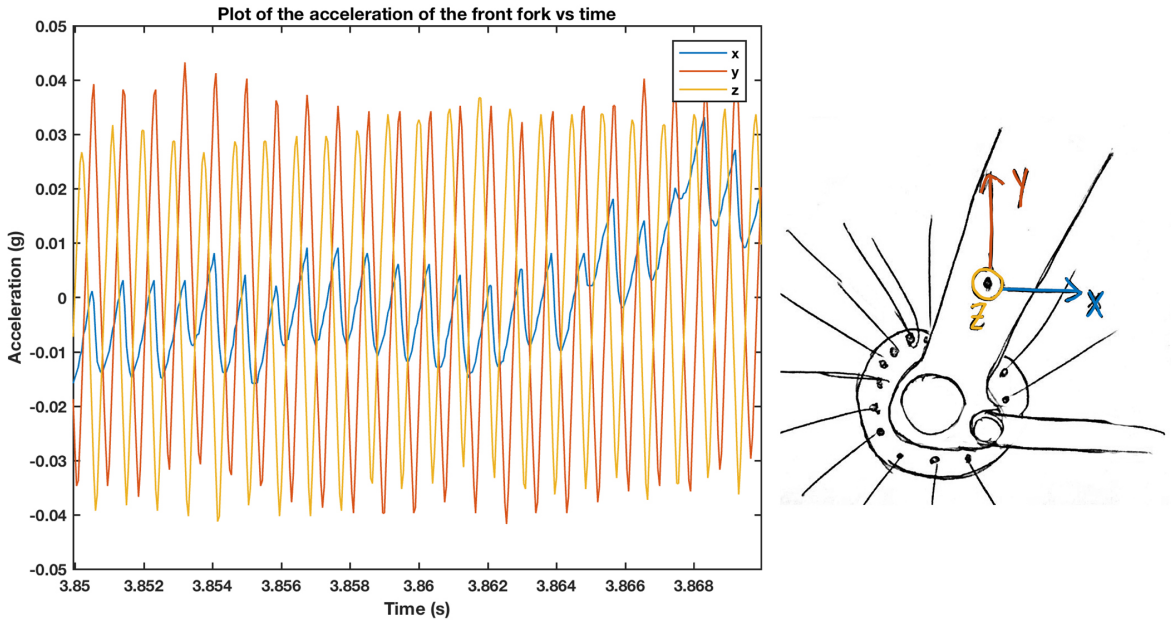

Figure 2.5: Results of the accelerometer attached to the front fork.

The vibrating frequencies of the front fork in each direction are:
f_x = 1120 f_y = 1116 Hz f_z = 1116 Hz.

Figure 2.6 shows the accelerometer results when attached to the the rim. Doing measurements with the accelerometer attached to the rim and spokes was a bit more challenging, because these are moving parts and the accelerometer is wired to a laptop. However, measuring only one rotation of the wheel is enough to get a decent amount of data.
It seems that the rim is also acting as a resonance box, because it is vibrating in all direction with frequency near the measured audio frequency. However, the amplitude in y-direction is smaller than amplitude in z-direction. This is possibly due to the fact that the rim is most stiff in y-direction.

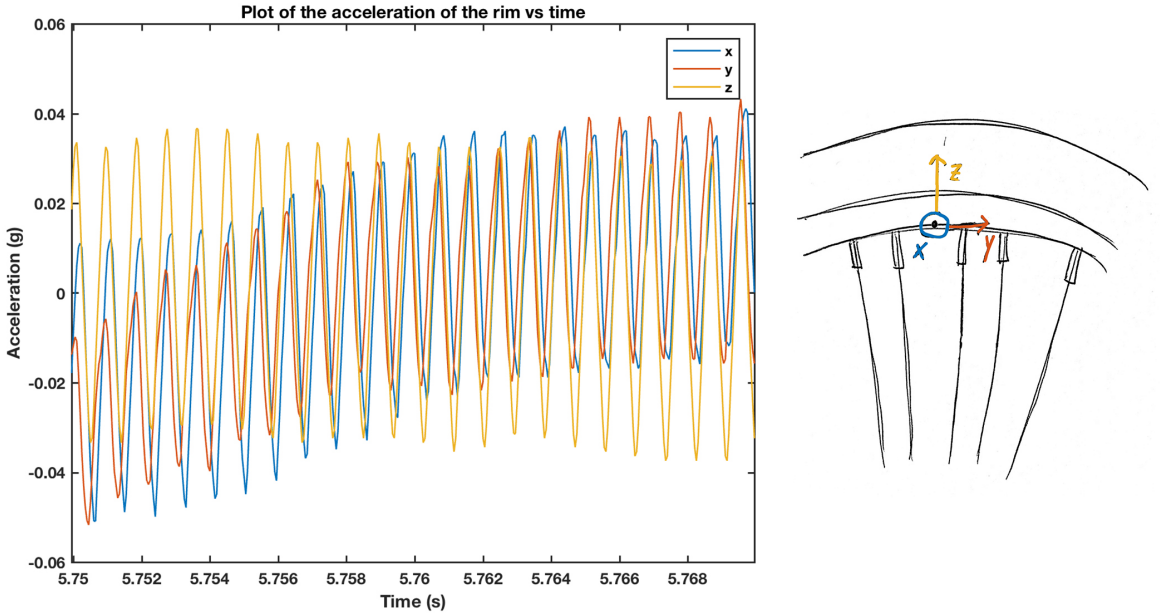

Figure 2.6: Results of the accelerometer attached to the rim.

From the FFT analysis it appeared that the vibrating frequencies of the rim are:
f_x = 1127 Hz f_y = 1127 Hz f_z = 1132 Hz.

Finally, the accelerometer is mounted to one of the spokes. The results are shown in figure 2.7. It can be concluded that the spokes are also vibrating in all direction with a frequency near the measure audio frequency. In this small portion of data the amplitude in x-direction is smaller then in y- and z-direction, but after running some other random samples of the data it appears that this is only a local effect.

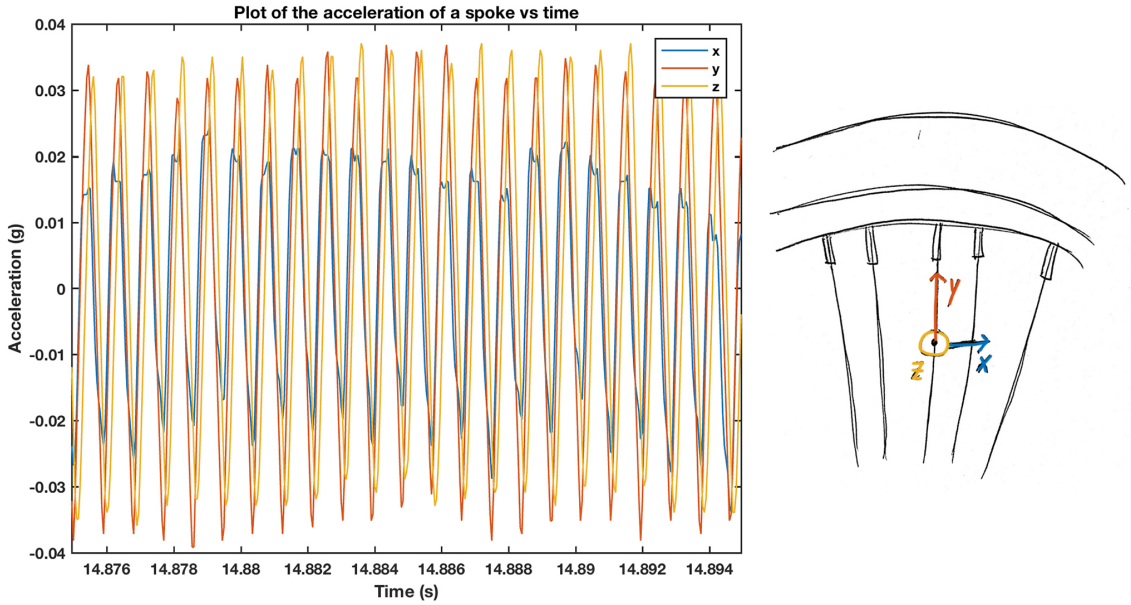

Figure 2.7: Results of the accelerometer attached to a spoke.

The FFT analysis showed that the vibrating frequencies in each direction are:
f_x = 1122 Hz f_y = 1122 Hz f_z = 1122 Hz.

2.1.3. Conclusion

From these first measurements can be concluded that all relevant bike parts are vibrating in nearly the same frequency as the measured audio frequency of the brake squeal. Furthermore, there are no clear differences in vibration amplitudes between the different bicycle parts. All amplitudes are around 0.04V.
It is surprising that there is no clear vibration in the x-direction of the front fork. Especially, because from other small experiments it appeared that bicycle with very stiff front forks don't squeal at all. Hopefully, measuring with the laser vibrometer will give more insight in the behavior of the front fork during brake squeal.
Furthermore, the vibration of the brake pad in z-direction indicate that stick-slip behavior of the brake pads is the cause of the friction induced vibration and therefore causing brake squeal.

2.2. Measurements with laser doppler vibrometer

The goal of the laser vibrometer measurements is not only to verify the results from the accelerometer but also to get more insight in the phenomenon of brake squeal. The advantage of a laser vibrometer is that it can measure the vibrating behavior of a surface by scanning the surface using a grid of measuring points. Hopefully this will show how the front fork is vibrating; in what kind of shape and directions. The laser vibrometer that will be used for this experiment is a Polytec PSV-400.

2.2.1. How a laser doppler vibrometer works

The working principle of a laser doppler vibrometer is based on the Doppler effect. The Doppler effect can easily be explained by the change in perceived frequency when an ambulance with sirens drives by. When there is a difference in velocity (magnitude or direction) between the sound source and the receiver, the perceived frequency changes [24]. When a laser beam with a certain frequency is reflected by a vibrating object, the frequency of the reflected laser beam is changed slightly. Also the phase of the wave will shift slightly. This change in frequency an phase gives information about the vibrating frequency and velocity of the object. The change of frequency (f_D) can be calculated as following [19]

$$f_D = 2 * \frac{v}{\lambda} \tag{2.1}$$

where v is the velocity of the object and λ the wavelength of the emitted wave. When the frequency shift and the wavelength of the emitted wave is known, the velocity of the vibrating object can be calculated. Due to the vibration, the measured velocity will constantly change from direction. Therefore, the velocity data will also give information about the frequency. In the case of a laser vibrometer the frequency shift is detected by the laser vibrometer. And the wavelength of the emitted light beam is also known. With this information the velocity and frequency of the vibrating object can be obtained.

The optical setup of the Polytec PSV-400

As mentioned before, a laser doppler vibrometer measures the frequency of a vibrating object based on the difference in frequency and phase of the emitted beam and the reflected beam. In order to do this, the emitted beam coming from the laser is splitted by a beam splitter (beam splitter 1) into a reference and a measurement beam (figure 2.9). The measurement beam is reflected by the object and sent to the detector via beam splitter 2. The reference beam is led to the detecter via a mirror and beam splitter 3. The Bragg cell (acousto-optic modulator) is added to determine the direction of the moving object. When the object is moving towards the laser it gives the same modulation pattern as when the object is moving in the opposite direction. The Bragg cell shifts the laser's light frequency with 40 MHz. The frequency of the laser light itself is $4.74 * 10^{14}$ Hz. When the object is at a standstill the modulation frequency of the interference pattern of the two light beams is 40 MHz. When the modulation frequency is more than 40 MHz it means that the object is moving towards the laser and when the measured modulation frequency is less than 40 MHz it means that the object is moving away form the laser. This means that is now possible to detect the direction of the movement [19].

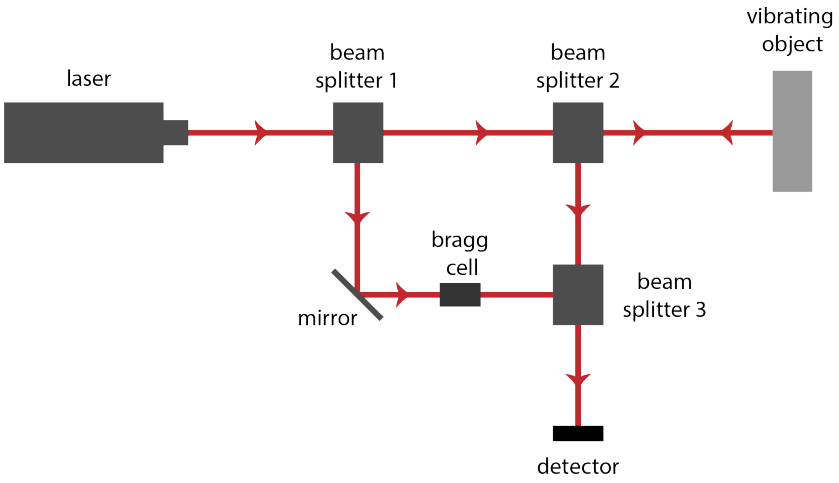

Figure 2.8: The optical setup of the Polytec PSV-400 [19].

Interferometry

At the detector, the measurement and the reference beam overlap and interfere. The phase and frequency difference between them creates a pattern of light and dark area's (interference fringes). The light area's are the places where the beams are in phase. The waves are added together an the light becomes brighter. The dark area's are the places where the beams are out of phase. From the obtained pattern, called an interferogram, the vibrating frequency of the object can be determined using a computer [3]. Also, using this pattern the amplitude of the vibrating motion can be determined. One cycle of dark and light area's correspondents to the wavelength of the light divided by two. This Polytec laser vibrometer uses a helium neon laser with a wavelength of 632 nm. This means that one cycle of dark and light area's is equal to 316 nm [19].

2.2.2. Experimental setup

Figure 2.9: Experimental setup to perform measurements with the laser doppler vibrometer.

The experiments are done without a person sitting on the saddle handling the bicycle. This way the experiments can be done with one person instead of two persons. A weight of 15 kg is added to the bicycle frame to keep the pressure of the front tire on the tread mill. The handlebar is fixed by two ropes (figure 2.10).

2.2.3. Experimental setup

Figure 2.10: Experimental setup to perform measurements with the laser doppler vibrometer.

2.2.4. Single point measurements

From the accelerometer measurement was concluded that all relevant bike parts are vibrating in nearly the same frequency as the measured audio frequency of the brake squeal. The laser vibrometer was used to do the same measurements in order to validate the accelerometer measurements. In contradiction to the accelerometer, the laser vibrometer measures velocity instead of acceleration.

Measurement procedure

First, at has to be made sure that the laser beam is perpendicular to the surface that has to be measured. After that, the laser beam has to be focused at the point of interest with the focusing button in the vibrometer software. After these two steps, the signal strength has to be checked. A signal strength of 20 percent is enough to get accurate results. Also, to increase the signal strength, aluminum tape is used. Aluminum tape improves the reflectivity of the material.

The next step is to choose the right settings in the Polytec software. The most important settings are the amount of measurements per point, bandwith, FFT lines and measurement range. For the single point measurements three measurements per point are sufficient. The software calculates the average after completing the three measurements. For the bandwith a range from 200 - 5000 Hz has been chosen to see if there are more vibration modes than just the main mode of approximately 1100 Hz. The amount of FFT lines influences the accuracy and the duration of the measurements. Less FFT lines give less accurate results, but reduces the duration time of the measurement. For the single point measurements the maximum amount of FFT lines of 6400 lines is chosen. This setting combined with a bandwith of 5000 Hz results in a measurement time of 1.2 s. The last setting is the velocity range in which the laser vibrometer should measure. Finding the right range is a process of trial and error. This process starts by choosing a small range. When the signal is out of range during the measurement, the range has to be increased. The Polytec software shows if the whether the signal is within the chosen range. For the measurements of this project, a maximum range of 1000 mm/s/V had to be used.

Results

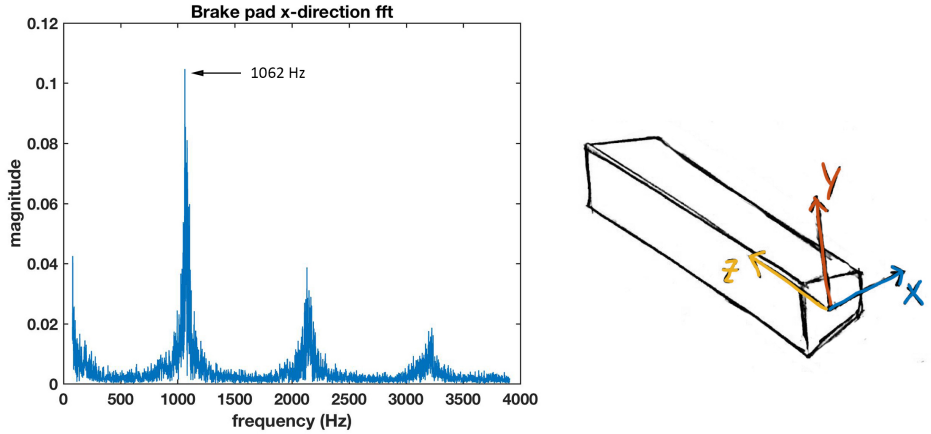

Figure 2.11: Single point measurement fft of the vibrating brake pad in x-direction.

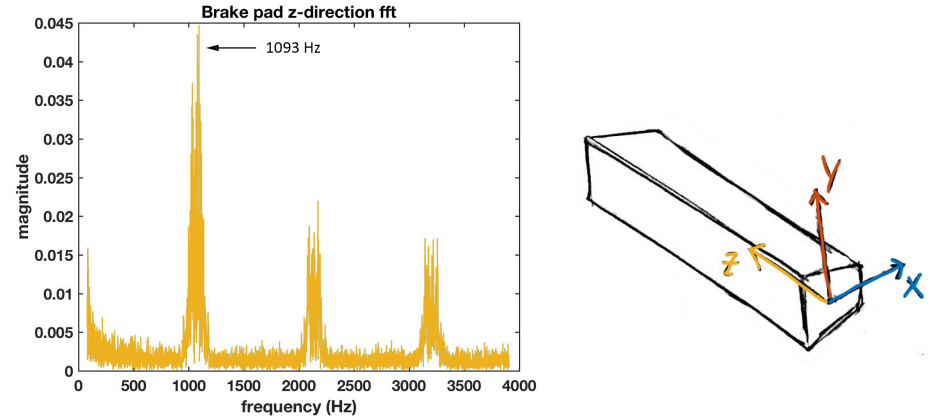

Figure 2.12: Single point measurement fft of the vibrating brake pad in z-direction.

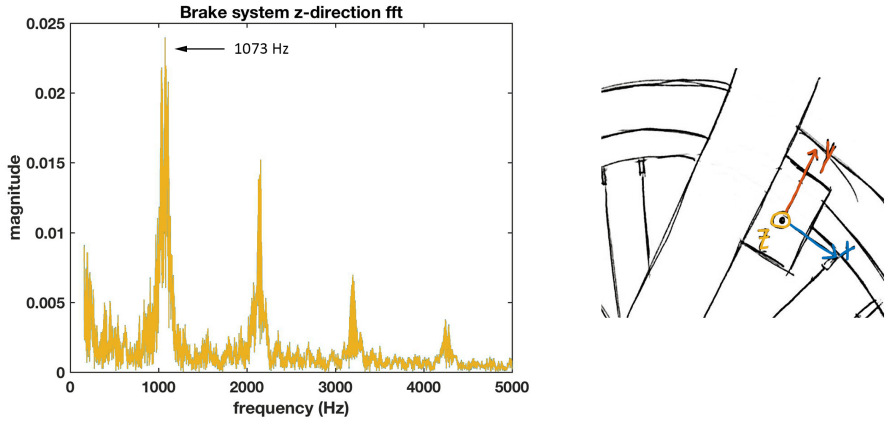

Figure 2.13: Single point measurement fft of the vibrating brake system in z-direction.

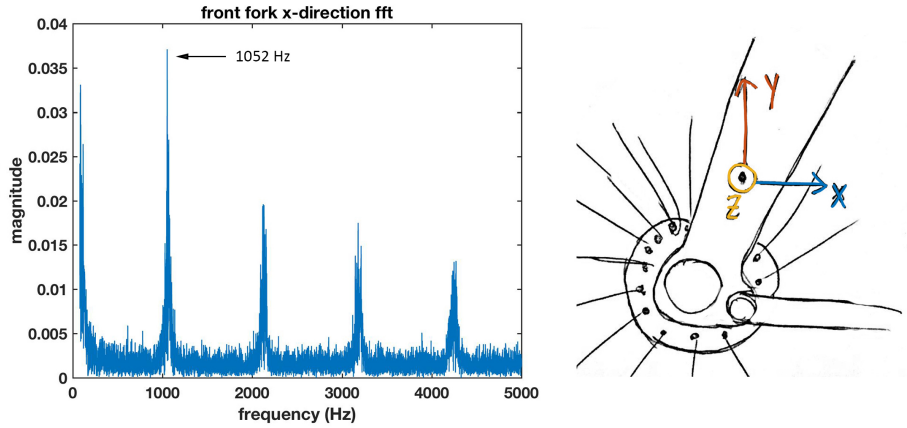

Figure 2.14: Single point measurement fft of the vibrating front fork in x-direction.

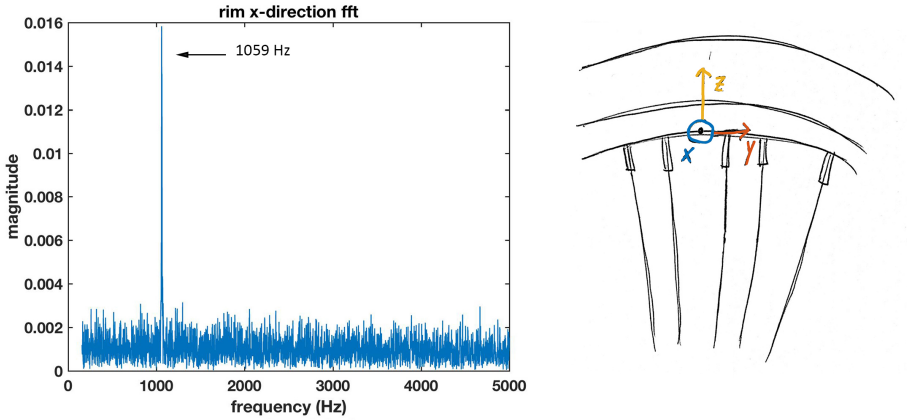

Figure 2.15: Single point measurement fft of the vibrating rim in x-direction.

The squeal noise was also recorded with an iPhone. The frequency was extracted from the audio file using Adobe Audition. The measured frequency was 1070 Hz.

2.2.5. Surface measurements

The main advantage of a laser vibrometer compared to an accelerometer is its ability to measure the vibrations of a whole surface. Surface measurements result in a 3D animation of the vibration modes of the surface. This will give more inside into the fundamental cause of bicycle brake squeal. The surface of the front fork will be scanned from the side and from the front. Also the rim will be scanned from the side. Doing these measurements is more complex than single point measurements.

Measurement procedure

1. The laser beam has to be more or less perpendicular to the surface of interest.

2. After autofocusing the laser the signal strength has to be at least 20 percent.

3. 2D alignment. The laser vibrometer software has to know where the laser point is on the screen. 2D alignment is done by moving the laser with three or four points on the screen and click on the laser point (figure 2.16a). After clicking, a blue marker is added to the screen.

4. Creating a grid (figure 2.16b). When the 2D alignment is done correctly the laser will follow the points on the grid accurately.
5. Selecting the mode for the animation.

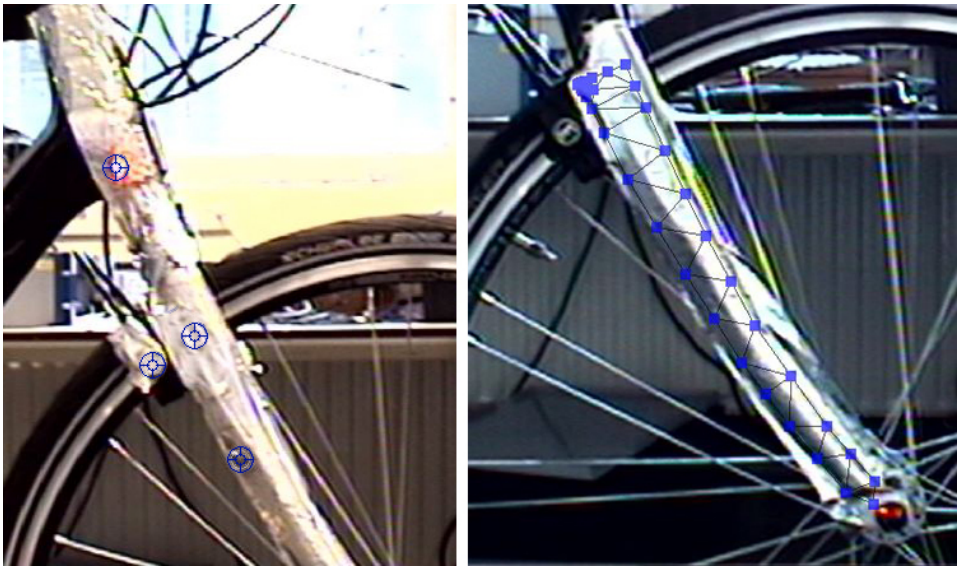

Figure 2.16: 2D alignment (a) and creating a scanning grid (b).

Results

Scanning the front fork from the side including a part of the headset

First the front fork and a part of the headset has been scanned by the laser vibrometer. A part of the headset was included to compare the front fork vibrations with the headset vibrations. On the very left side of figure 2.17 the grid is shown that is used to scan the surface. Some frames of the animation are shown in figure 2.17.

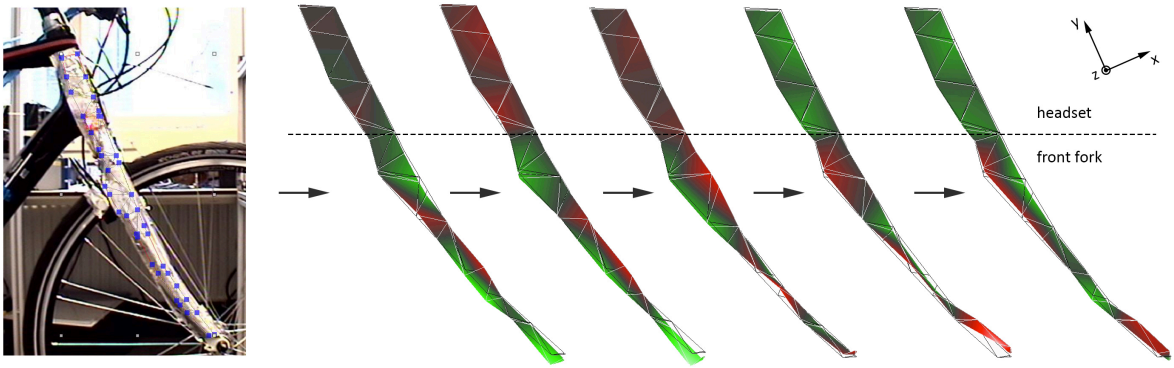

Figure 2.17: Results of scanning the front fork from the side.

For the animation the squeal mode of 1070 Hz is chosen, because this mode matches the audio frequency of the squealing. Also this mode has the biggest peak in the FFT graph. From the animation can be concluded that the deformation of the front fork is combination of deformation in the out-of-plane direction (z-direction) and torsion around the y-axis. The deformation of the headset shows only vibration in the out-of-plane direction (z-direction). In figure 2.17 the color of the headset surface changes in its entirety from red to green, indicating that the surface is just vibrating in the z-direction. The out-of-plane vibrations of the front fork and headset indicate that they are functioning as resonance boxes amplifying the vibrations coming from the brake pads. However, the torsional vibrations of the front fork

show that the torsional stiffness of the front fork is probably an important factor. Furthermore, note that the bottom of the front fork barely moves in the x-direction. Apparently, the front fork barely vibrates in the x-direction. This also confirms the measurements results from the accelerometer (figure 2.5).

Adding a brake booster to the brake system

Adding a Magura brake booster increases the stiffness of the front fork.

Figure 2.18: Magura brake system with a brake booster.

The scanning results are shown in figure 2.19.

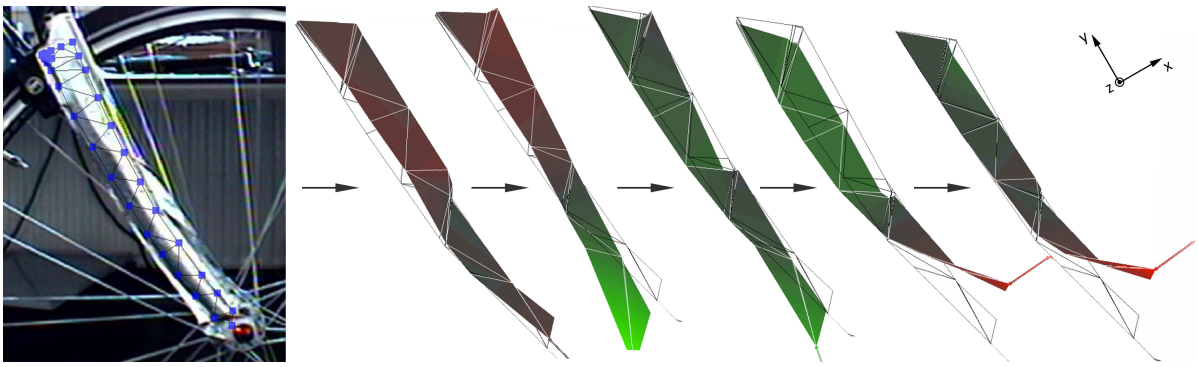

Figure 2.19: Results of scanning the front fork (with bracket) from the side.

With the bracket added to the brake system, the bicycle is not squealing anymore. Also, in the FFT graph there are no clear modes visible. However, to compare this animation with the previous one, the same mode of 1070 Hz is chosen. In the animation of vibrating front fork can be seen that the torsional vibration is gone, while the out-of-plane vibration is still present. Apparently, the torsional vibration causes the brake squeal.

Scanning the front fork from the front

Scanning the front fork from the front gives similar results as scanning it from the side. Again the animation shows a deformation that is a combination of deformation in the out-of-plane direction (z-direction) and torsion around the y-axis. The results is shown in figure 2.20.

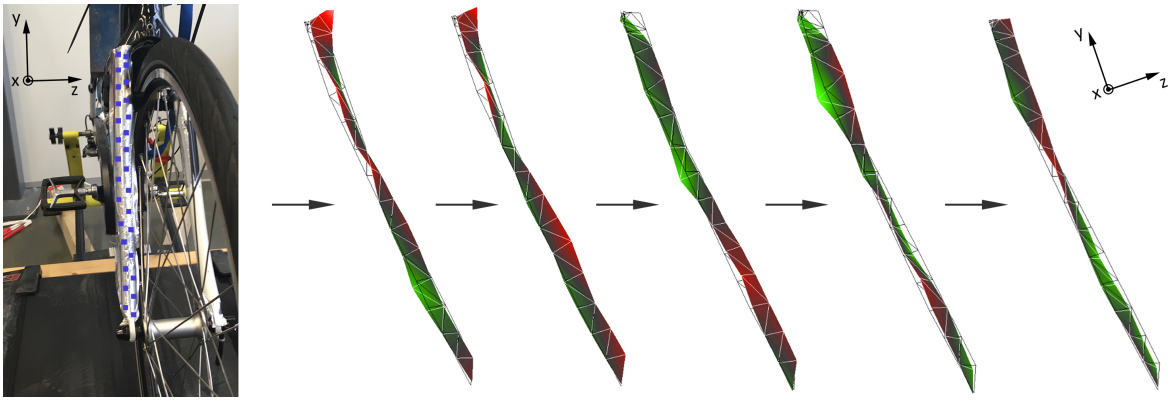

Figure 2.20: Results of scanning the front fork from the front.

Scanning the rim

The front rim was scanned from the side. The very left side of figure 2.21 shows the scanning grid that is used. The animation shows out-of-plane vibrations of the rim with the same frequency as the squeal frequency. The vibration mode at this frequency consists of 6 nodes. Also, the amplitude of the vibration is bigger at the area of the brake pad than at the bottom part of the rim. This makes sense, because the friction of the brake pads induces the vibration of the rim. Also, the vibration are damped at the bottom of the rim, due to the contact point of the tire and the tread mill.

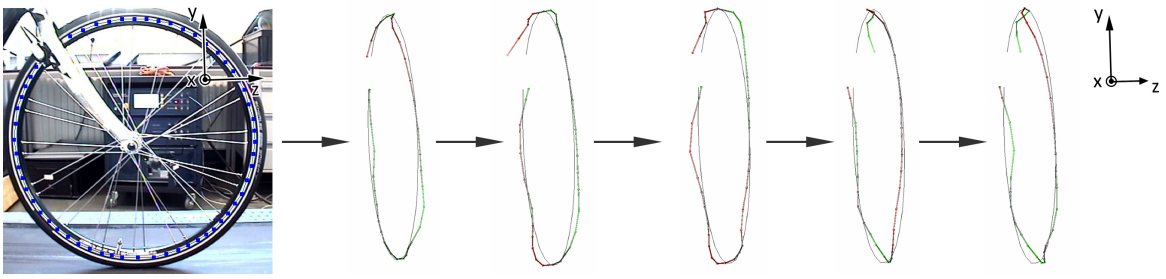

Figure 2.21: Results of scanning the front fork from the side.

2.3. Discussion and Conclusion

Like the previous measurements performed with the accelerometer, the vibration frequencies of the different bicycle parts are nearly the same as the frequency extracted from the audio file. The measured bicycle parts include the brake system (holding the brake pads), the brake pads themselves, the rim, the spokes and the front fork. However, the measured frequencies in this experiment are approximately 50-60 Hz lower than the measured frequencies with the accelerometer experiment. This has probably to do with the change of the front hub. The original wheel had to be replaced, because the bicycle was not squealing anymore. The same rim, spokes and tire was used, but the original front hub was not available anymore. This new front hub probably changed the mass and stiffness of the system slightly.

The vibration animations of the front fork gave a lot more insight in the fundamental cause of brake squeal. The most important and also surprising conclusion is that the front fork is vibrating in torsional direction (around z-axis) rather than in the xy-plane. This was also confirmed by the accelerometer results (figure 2.5). Furthermore, after adding a Magura brake booster to the brake system the squealing and the torsional deformations of the front fork were gone. Apparently the stiffness of the front fork is a key factor when it comes to bicycle brake squeal.

3

Potential squeal parameters

Brake squeal is known as a very capricious problem. Brake squeal can magically appear and disappear over time. When a brake system squeals one day, it doesn't mean it will squeal the next day. This is due to the high complexity of the problem. A lot of variables are involved. When one variable changes, squeal propensity can suddenly increase or sometimes just disappear. A well known example is rainy weather. Rain and dirt can increase squeal propensity for some bicycles. Another example is the wear of the brake pads. Most brand new bicycles don't squeal in the first few months. However, due to wear of the brake pads and the rim, over time brake squeal can become a problem.
Figure 3.1 shows all potential squeal parameters. The potential parameters are divided in three groups: fork, wheel and brake system. In total there are 17 potential parameters. Unfortunately, it is not possible to study the contribution of all these parameters in brake squeal separately, therefore we will focus on the most important parameters only.

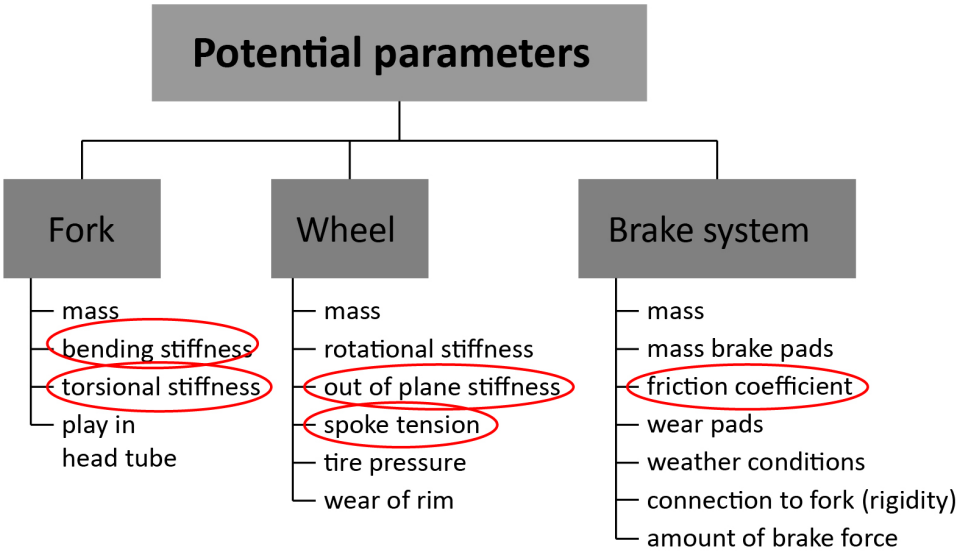

Figure 3.1: Parameters that may contribute to squeal propensity during braking

The first parameter that will be studied is the friction coefficient of the brake pad and the rim. As discussed earlier, brake squeal is caused by friction induced vibration. Therefore, it's important to study the influence of the friction coefficient on brake squeal.

Another important parameter is the fork stiffness, both bending and torsion stiffness. From the first measurements (H2) it was concluded that the front fork is vibrating in torsional direction. This indicates that torsional stiffness of the front fork is an important factor

when it comes to brake squeal. Also, from some little trial and error experiments it appeared that changing the front fork changed the squeal propensity and also the squeal frequency.

The third parameter that will be studied is the spoke tension. According to a study of Nakae et al. [15] spoke tension influences the squeal frequencies. In this study a mountainbike with disc brakes is used as research object. Also, changing the spoke tension will change the out-of-plane stiffness of the rim and therefore also its vibrating behavior.

These five parameters will be studied in the next three chapters.

4

Front fork stiffness

The first potential squeal parameter we will zoom into is the front fork stiffness. From some trial and error experiments it appeared that changing the front fork of the bicycle influenced the squeal frequency. Probably this is due to differences in fork stiffnesses. There are more types of fork stiffnesses in different directions. To find the stiffnesses which are important during braking, it's necessary to start with a force analysis.

In figure 4.1a a free body diagram (FBD) is drawn of the front wheel and front fork. The body connected to the front fork represents the rest of the bicycle including the driver. During braking the inertia force ($F_{inertia}$) is the driving force and causes the front wheel to rotate counter clockwise.

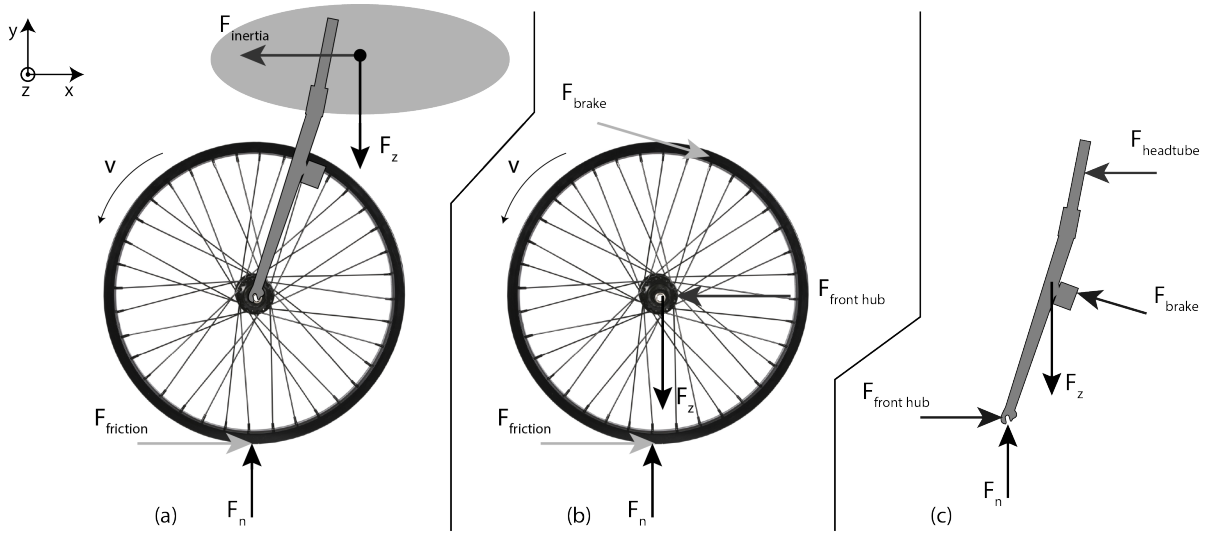

Figure 4.1: A FBD of the whole system (a), wheel isolated (b) and front fork isolated (c)

Figure 4.1b shows a force analysis of the front wheel. The brake force F_{brake} directed in the opposite direction of the rotating velocity of the wheel. During braking the braking force is bigger than the friction force causing the rotating wheel to slow down. To keep the wheel in equilibrium in x-direction, the force on the front hub has to be in the negative x-direction. This means also that the force on the pads of the front fork has to be in opposite direction (figure 4.1c), according to Newtons third law. The same principle applies to the brake force. From this force analysis can be concluded that the bending of the front fork in xy-plane is caused by the force of the front hub to the front fork pads ($F_{fronthub}$).

Most forces take place in the xy-plane, however the normal force of the brake pad ($F_{n,brakepad}$) is directed in the z-direction. This force is further analyzed in figure 4.2.

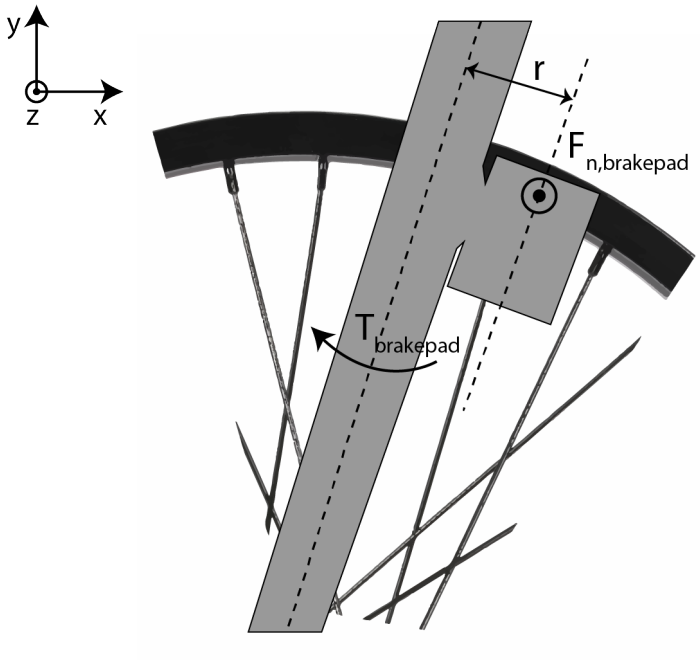

Figure 4.2: A force analysis of the brake pad normal force

The normal force of the brake pads causes torsion ($T_{brakedpad}$) of front fork legs, where $T_{brakepad} = F_{n,brakepad} * r$.

From the force analysis can be concluded that there are two types of front fork stiffnesses which are important for brake squeal: bending stiffness and torsional stiffness. These two stiffnesses are defined in figure 4.3.

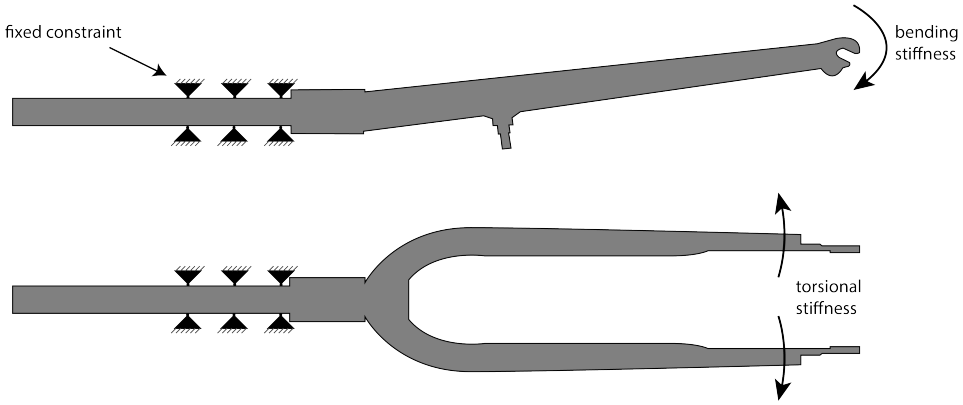

Figure 4.3: Definition of front fork bending stiffness and torsional stiffness

The four front forks that will be measured

The four front forks that will be used in this experiment are shown in figure 4.4. These forks are chosen and provided by the Koninklijke Gazelle.

4.1. Measuring bending stiffness

To measure the bending stiffness, the fork is clamped into a vise at the point where the fork goes into the head tube. It is assumed that there is no play between the fork and the head tube. In this case the head tube functions as a fixed constraint. In this experiment, the vise represents the fixed constraint of the head tube. At the other end of the fork there is a weight applied that represents the force on the front hub to the front fork pads (figure 4.1c). At the

Figure 4.4: The four different front forks that will be used in this experiment

same point the weight is attached, a dial indicator is placed to measure the displacement. A relative low weight of 6 kg is used to make sure the deformations stay in the linear area. At the same time 6 kg is enough to get decent measurements with the accuracy of 0.01 mm with the SARRA dial indicator. The magnetic stand of the dial indicator is attached to a metal plate to eliminate any movement. The experimental setup is shown in figure 4.5.

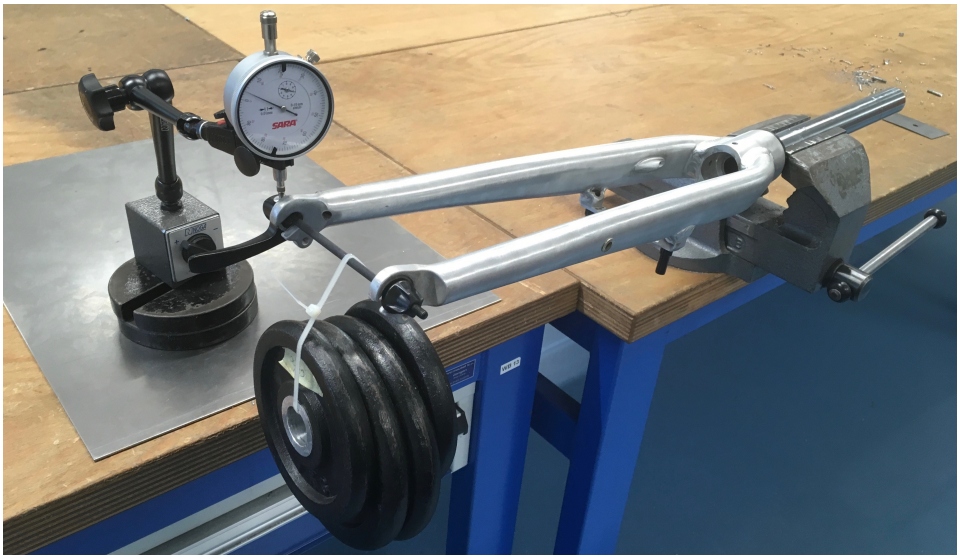

Figure 4.5: Experimental setup to measure front fork bending stiffness

The dial indicator is placed at the center of the quick release mechanism to make sure that the length to the fixed end of the fork is the same for the weight as for the weight attachment. After clamping the fork into the vise, the displacement is measured at the other site of the vise. This is done to make sure that there is no movement at the fixed end of the fork (figure 4.6).

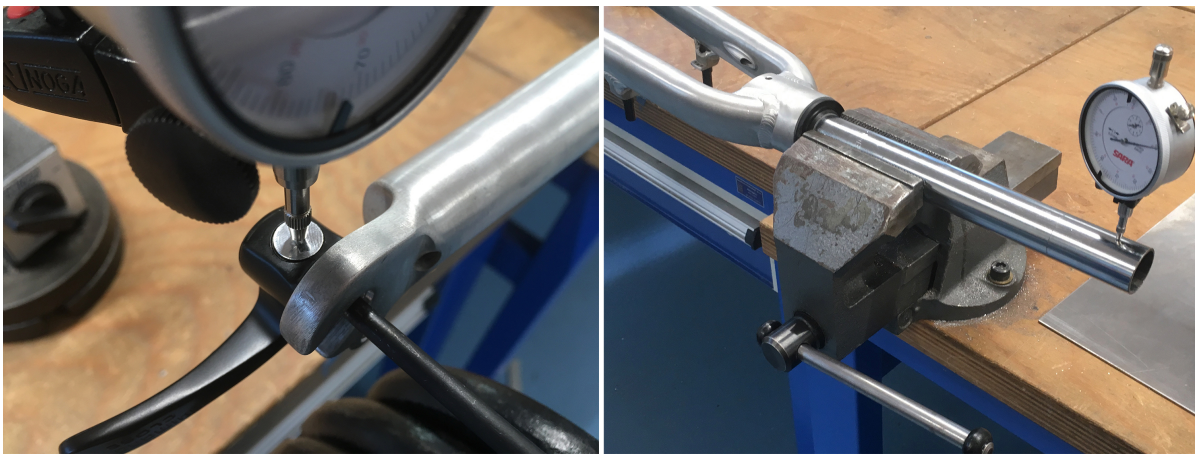

Figure 4.6: Dial indicator placement (left) and make sure method of clamping is correct (right)

The distance between the quick release clamp and the fixed end of the fork is measured using a tapeline. The perpendicular distance is determined by taking a side view picture of the fork and measure the length of $l_{perpendicular}$ and $l_{measured}$ in pixels. Using these lengths the ratio between these lengths can be calculated and thereby the perpendicular distance in mm. This is done for each fork separately, since each fork has another shape. Using this perpendicular distance, the moment applied to the fork and the deformation angle can be calculated (figure 4.7).

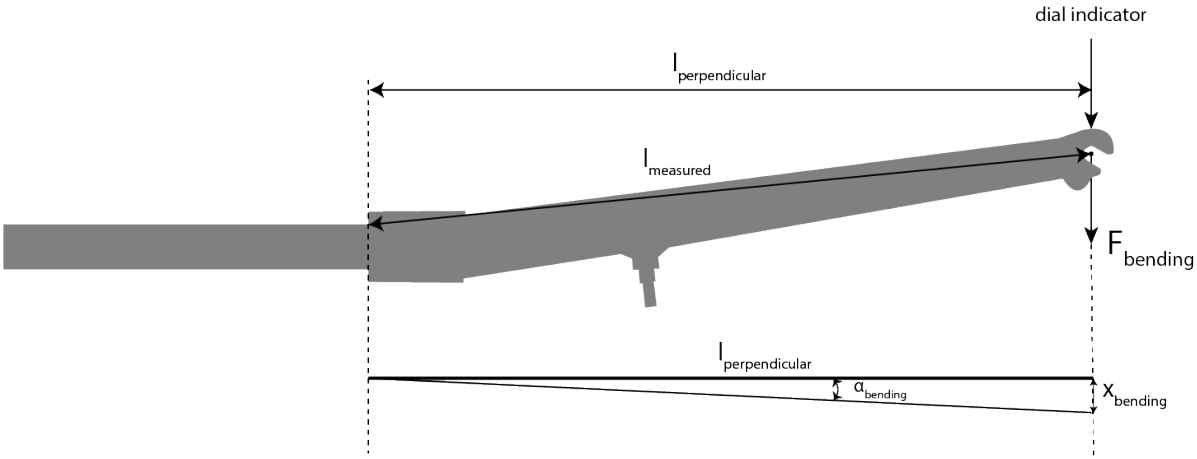

Figure 4.7: Fork measurements and angle of deformation

The moment applied to the fork is

$$M_{bending} = m * g * l_{perpendicular}, \tag{4.1}$$

where m is 6 kg, g is 9.81 m/s^2 and $l_{perpendicular}$ is fork dependent.

The angle of deformation is

$$\alpha_{bending} = tan^{-1}\left(\frac{x_{bending}}{l_{perpendicular}}\right) \tag{4.2}$$

where $x_{bending}$ is the measured displacement.

Now the bending stiffness can be calculated by dividing the applied moment by the angle of deformation:

$$k_{bending} = \frac{M_{bending}}{\alpha_{bending}}. \tag{4.3}$$

Results

For each fork, four measurements have been done to increase accuracy. For each measurement the dial indicator was replaced on the same position. The results are shown in table 4.1.

Table 4.1: Results of the front fork bending stiffness experiment

	$x_{bending}$ (mm) Al. (silver)	$x_{bending}$ (mm) Al. (black)	$x_{bending}$ (mm) Carbon	$x_{bending}$ (mm) Steel
Measurement 1	0.66	0.95	0.86	0.62
Measurement 2	0.60	0.96	0.83	0.63
Measurement 3	0.58	0.97	0.84	0.72
Measurement 4	0.61	0.99	0.82	0.67
Average	0.61	0.97	0.84	0.66

The next table (table 4.2) shows the average measured displacement (from previous table), the perpendicular distance $l_{perpendicular}$ as defined earlier, the moment applied to the forks and finally the calculated bending stiffness $k_{bending}$ in $Nm/^o$.

Table 4.2: Results of the front fork bending stiffness experiment

	$x_{bending}$ average (mm)	$l_{perpendicular}$ (mm)	$\alpha_{bending}$ (^{o})	Applied moment (Nm)	$k_{bending}$ ($Nm/^o$)
Al. (silver)	0.61	451	0.08	27	341
Al. (black)	0.97	474	0.12	28	239
Carbon	0.84	421	0.11	25	217
Steel	0.66	454	0.08	27	320

4.2. Measuring torsional stiffness

To measure the torsional stiffness of the front fork, weights are attached via threaded rods, connected to the pads at the lower end of the fork. The weights are applied in a symmetrical way (figure 4.8), because in a real braking scenario the fork is also loaded symmetrically.

Another advantage of keeping the setup symmetrical is that place of clamping becomes irrelevant as long as it is at the upper part of the fork. Because, from the point where both legs of the fork meet each other, the netto torsion becomes zero.

In order to measure the torsion of the front fork leg without measuring the deformation of the threaded rod, it's important to separate the point of measuring from the point of applying the load. Therefore, a metal profile is used to measure the displacement caused by the torsion of the fork leg. Furthermore, another measurement has to be done at the pad of the fork to measure bending of the fork caused by the weight (4.9). Subtracting the bending displacement from the torsion displacement gives pure torsional displacement (4.10).

A schematic representation of the setup is shown in figure (4.10). A weight of 2.5 kg is used on both sides. The distance to the applied load is measured from the center of front fork pad.

The moment applied to the front fork leg is

$$M_{torsion} = m * g * d_2 \tag{4.4}$$

where m is 2.5 kg, g is 9.81 m/s^2 and d_2 is 173 mm.

The angle of deformation is

$$\alpha_{torsion} = tan^{-1}(\frac{x_{torsion}}{d_1}), \tag{4.5}$$

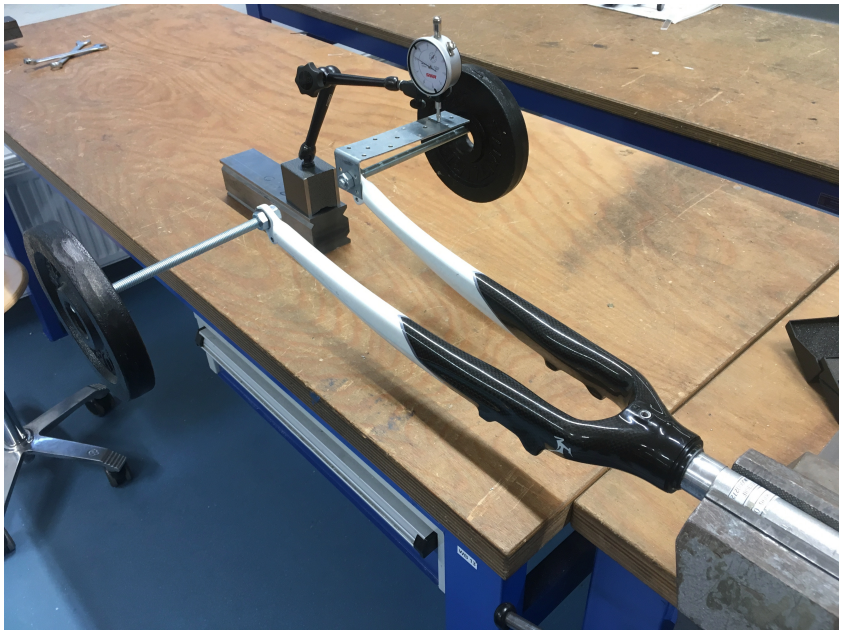

Figure 4.8: Test setup for measuring the torsional stiffness with symmetrical loading.

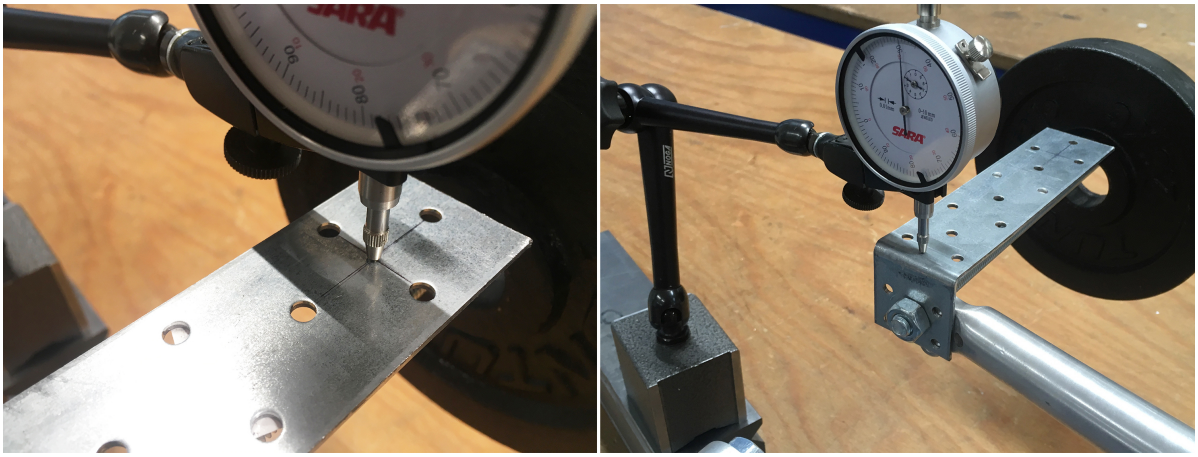

Figure 4.9: Measuring torsional displacement (left) and bending displacement (right).

where $x_{torsion}$ is the measured displacement.

Now the torsion stiffness can be calculated by dividing the applied moment by the angle of deformation:

$$k_{torsion} = \frac{M_{torsion}}{\alpha_{torsion}}. \tag{4.6}$$

Results

The experiment is done with and without bracket (figure 4.11).

Results with bracket

Table 4.3 shows the measurements for the netto displacement (position 2 extracted from position 1). (figure 4.10). For each measurement the dial indicator was replaced at the same position.

The lengths $d_1 = 122mm$ and $d_2 = 173mm$ are constants for all forks. $F_{torsion}$ can be calculated by multiplying the mass of 2.5 kg by the gravitational constant: $F_{torsion} = 2.5{*}9.81 = 24.5N$. Table 4.4 shows the average torsion displacement ($x_{torsion}$), the applied moment, the torsion angle ($\alpha_{torsion}$) and the torsion stiffness ($k_{torsion}$).

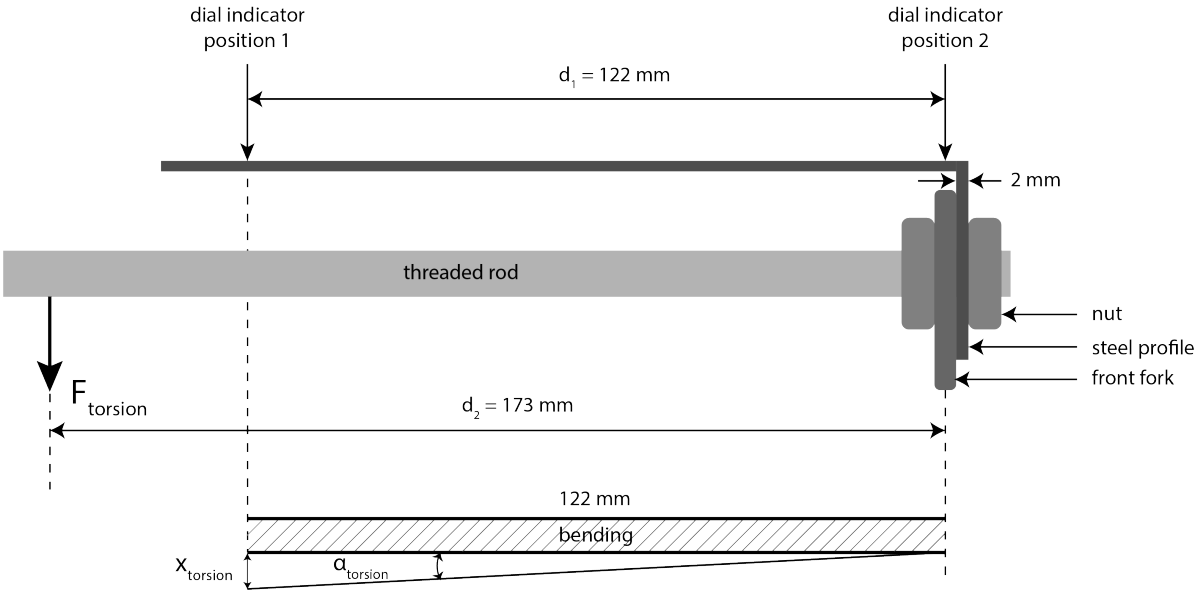

Figure 4.10: Schematic representation of the test setup.

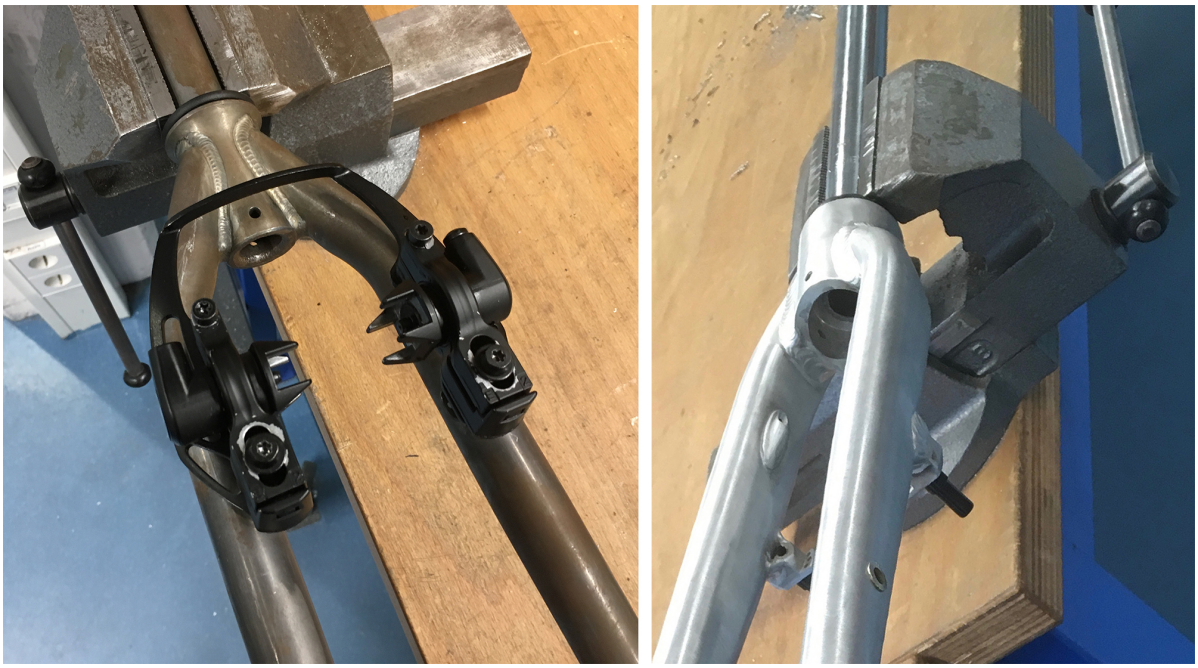

Figure 4.11: Front fork with (left) and without bracket (right).

Table 4.3: Results of the front fork torsion stiffness (with bracket) experiment

	$x_{torsion}$ (mm) Al. (silver)	$x_{torsion}$ (mm) Al. (black)	$x_{torsion}$ (mm) Carbon	$x_{torsion}$ (mm) Steel
Measurement 1	0.26	0.37	0.83	0.28
Measurement 2	0.26	0.34	0.83	0.28
Measurement 3	0.29	0.33	0.86	0.25
Measurement 4	0.27	0.32	0.83	0.24
Average	0.27	0.34	0.84	0.26

Table 4.4: Results of the front fork bending stiffness experiment

	$x_{torsion}$ average (mm)	$\alpha_{torsion}$ (^{o})	Applied moment (Nm)	$k_{torsion}$ ($Nm/^o$)
Al. (silver)	0.27	0.13	4.24	33.5
Al. (black)	0.34	0.16	4.24	26.6
Carbon	0.84	0.39	4.24	10.8
Steel	0.26	0.12	4.24	34.7

Results without bracket

Table 4.5 shows the measurements for the netto displacement (position 2 extracted from position 1). (figure 4.10).

Table 4.5: Results of the front fork torsion stiffness (without bracket) experiment

	$x_{torsion}$ (mm) Al. (silver)	$x_{torsion}$ (mm) Al. (black)	$x_{torsion}$ (mm) Carbon	$x_{torsion}$ (mm) Steel
Measurement 1	0.26	0.29	0.75	0.33
Measurement 2	0.28	0.29	0.78	0.27
Measurement 3	0.28	0.29	0.85	0.35
Measurement 4	0.25	0.26	0.83	0.35
Average	0.27	0.28	0.80	0.33

Table 4.6 shows the average torsion displacement ($x_{torsion}$), the applied moment, the torsion angle ($\alpha_{torsion}$) and the torsion stiffness ($k_torsion$).

Table 4.6: Results of the front fork bending stiffness experiment

	$x_{torsion}$ average (mm)	$\alpha_{torsion}$ (^{o})	Applied moment (Nm)	$k_{torsion}$ ($Nm/^o$)
Al. (silver)	0.27	0.13	4.24	33.5
Al. (black)	0.28	0.13	4.24	32.5
Carbon	0.80	0.38	4.24	11.3
Steel	0.33	0.15	4.24	27.4

4.2.1. Measuring the squeal frequencies of the front forks

Figure 4.12 shows the measured audio recorded with an iPhone during brake squeal. As can be seen in the graphs the carbon fork is squealing continuously, while the black aluminum fork squeal only short periods of time. The silver aluminum fork is barely squealing and the steel fork is not squealing at all. During the measurements the brake force was varied by hand to get as much squeal audio as possible. The squeal frequencies are extracted from the audio files by using Adobe Audition.

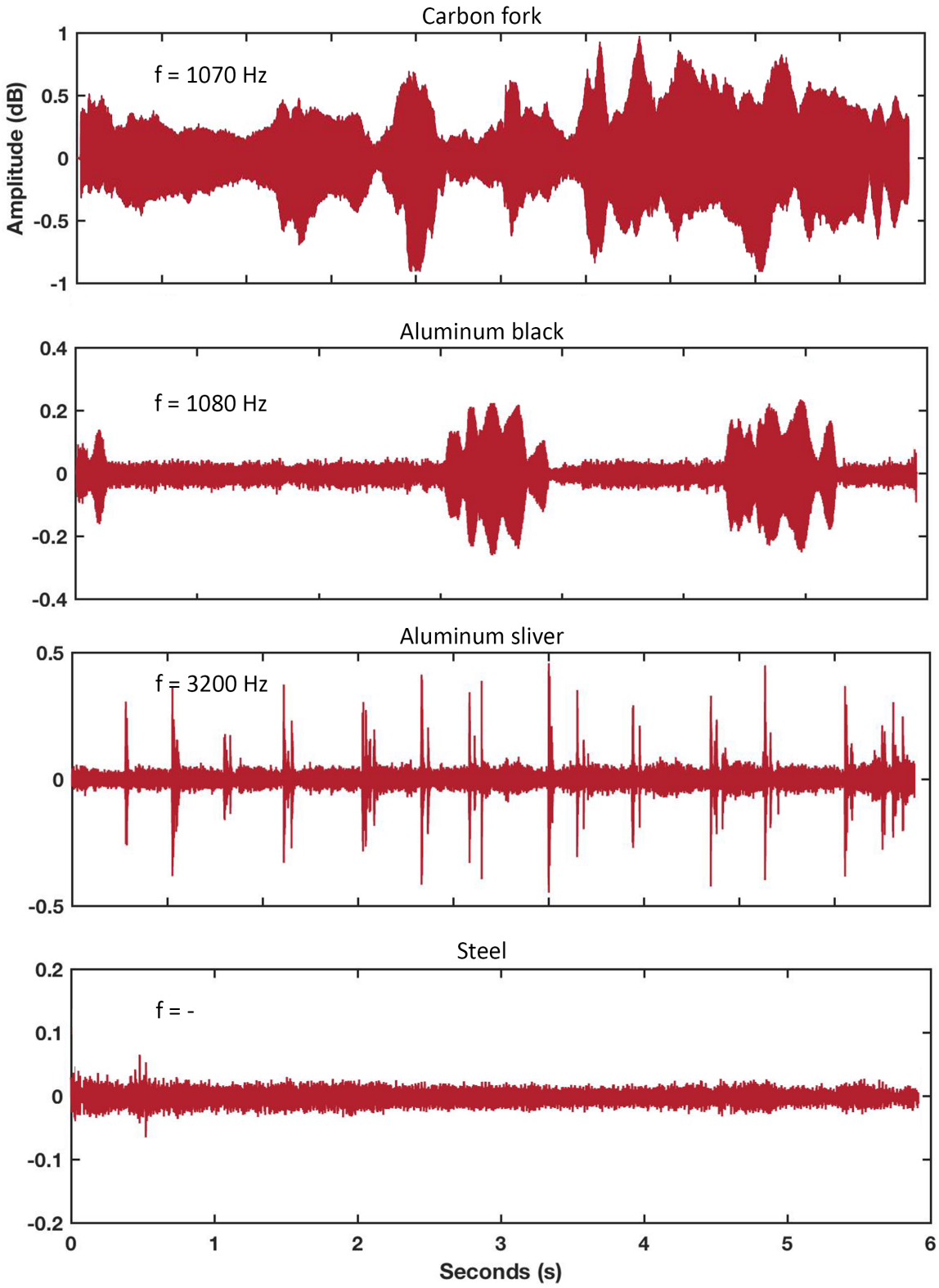

Figure 4.12: Recorded audio of the four different front forks during brake squeal.

4.3. Discussion and Conclusion

Table 4.7 shows an overview of the masses, the bending stiffnesses and the torsion stiffnesses of the forks. The carbon fork has the lowest stiffness for bending and torsion, especially for torsion. The carbon fork is also by far the lightest fork. However, the heaviest fork (steel) is not the most stiff fork for bending. Still, there seems a connection between the weight of the fork and it's bending and torsion stiffness. Furthermore, adding the bracket to the front fork doesn't really change the torsional stiffness of the front fork. Probably it does add stiffness, but the added stiffness is negligible to the torsional stiffness of the front fork.

Table 4.7: An overview of the stiffnessess and masses of the forks.

	mass (kg)	$k_{bending}$ $(Nm/^o)$	$k_{torsion}$ $(Nm/^o)$ with bracket	$k_{torsion}$ $(Nm/^o)$ without bracket	f (Hz)
Al. (silver)	1.07	341	33.5	33.5	3200
Al. (black)	1.27	239	26.6	32.5	1085
Carbon	0.56	217	10.8	11.3	1065
Steel	1.45	320	34.7	34.7	-

Discussion

The results of the laser vibrometer measurement (Chapter 2) showed that the front fork was vibrating in torsional direction during brake squeal. After adding a brake booster (bracket) the squealing and the torsional vibrations were gone. However, the results of the torsion stiffness's don't show clear differences of the torsion stiffness when the bracket is added. In other words, the results of the laser vibrometer and the results of torsion stiffness measurement seem to contradict. Maybe this is due to the fact that the main function of the brake booster is to make the brake system stiffer in torsional and outward direction. When the brake booster prevents the brake system from vibrating, the vibration won't be handed over to the front fork and therefore prevent the front fork from vibrating in torsional direction. Another explanation for this contradiction is that the method of measuring the torsional stiffness is not correct. Because in reality the forces are applied differently to the the front fork. The pads at the lower end of the fork are rigidly connected to each other by the front hub and the torsion force is not applied to the pads of the fork but at the point were the brake pads press against the rim. However, the method used in this experiment should be sufficient to compare the relative torsional stiffness's of the different front forks.

Another important thing to note is that changing the front fork changes three different parameters at ones: mass, bending stiffness and torsional stiffness. To accurately study one parameter, the other parameter have to be kept constant. This makes it harder to draw meaningful conclusions from this experiment.

5

Friction coefficient

As discussed earlier, brake squeal is most likely caused by stick-slip. Stick-slip occurs when there is a relative large difference between the static and kinetic friction coefficient. Therefore, it's important to study the influence of the static and kinetic friction coefficient on squeal propensity.

5.1. Experimental setup

There are different ways to measure the friction coefficient between the brake pad material and the rim material. The most easy way is to leave the brake pads and the rim in the original assembly of the bicycle. This will also give more realistic results than testing the friction materials independently from the bicycle, because this way the real braking scenario is better simulated. According to friction law of Coulomb the friction coefficient can be calculated by dividing the friction force (F_f) by the normal force (F_n) exerted on the object [26].

$$\mu = \frac{F_f}{F_n} \tag{5.1}$$

In the case of braking, the normal force is the force of the brake pads exerting on the rim and the friction force is the force between the brake pads and the rim in the opposite direction of the rotating rim direction. The static friction force (μ_s) can be measured when the friction force force and the driving force are the same. The kinetic friction coefficient (μ_k) can be calculated when the driving force of the wheel is bigger than the friction force from the brake pads, causing the rim to rotate with a constant velocity. However, measuring the friction coefficient in the bicycle assembly makes it harder to measure the force of the brake pads exerting on the rim. Therefore, instead of measuring force, the oil pressure in the hydraulic system of the brake will be measured. The measured oil pressure will give an indication of the force of the brake pads on the rim. Obviously, this method will not give absolute results. However, there exists a linear relation between pressure and force:

$$P = \frac{F}{A} \tag{5.2}$$

In addition, when the contact area (A) of the brake fluid with the brake piston is known, the brake force can easily be calculated. Otherwise, comparing the relative friction coefficients of the different types of brake pads will give enough information to draw some conclusions. The experimental setup that is used for this experiment is shown in figure 6.1.

The bicycle is clamped in a bicycle stand. A weight is used as a driving force of the wheel and is connected with a chord to the wheel with the same distance (r) from the front hub as the brake pads. The pressure sensor is connected to the hydraulic circuit of the brake system.

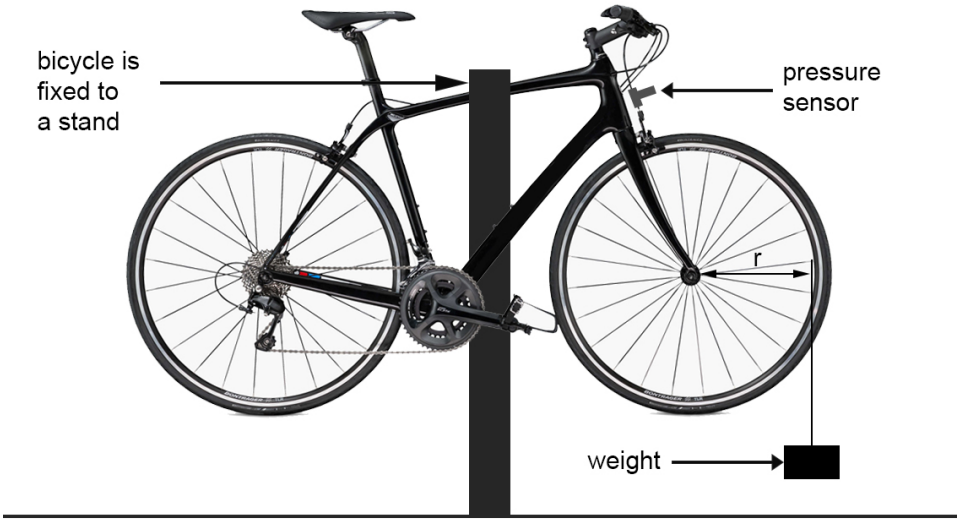

Figure 5.1: The experimental setup to measure the friction coefficient of various types of brake pads.

Pressure sensor

Figure 5.2a shows a schematic representation of the working principle of hydraulic brakes. During braking, pinching the brake handle causes the master piston of the hydraulic system to move. Due to the incompressible property of brake fluid, the moving force in the master piston will be translated to the two slave pistons, which are connected to the brake pads. The exerted force on the master piston is distributed over the two slave pistons.

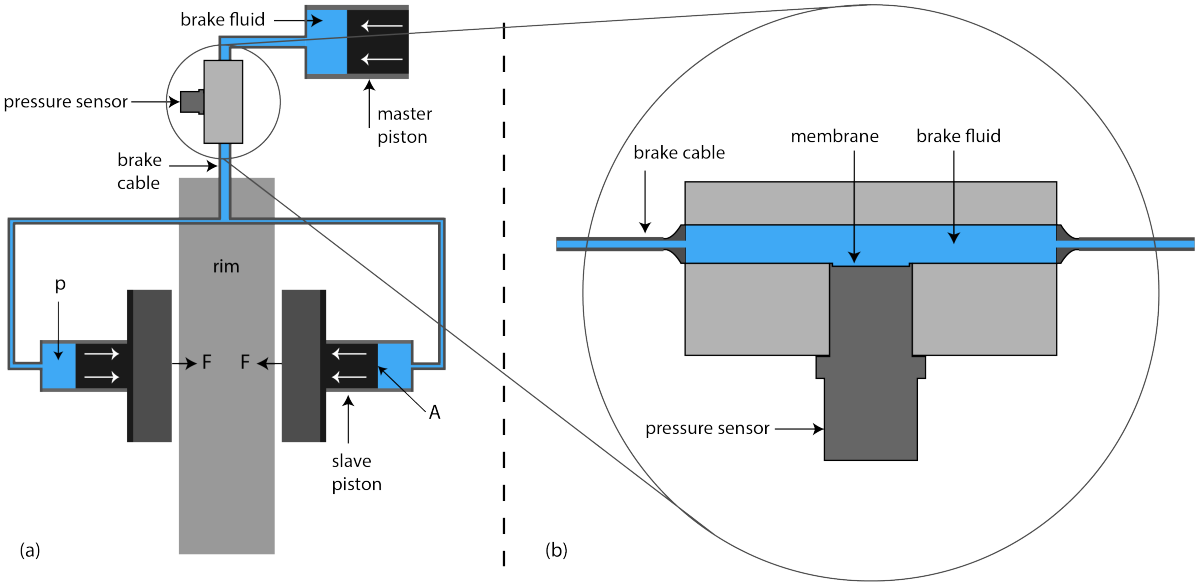

Figure 5.2: A schematic representation of the working principle of hydraulic brakes (a) and the cross section of the design of an aluminum block that connects the pressure sensor to the hydraulic circuit (b).

The pressure sensor is connected to the hydraulic circuit by a small aluminum block that is designed specifically for this experiment. This design is shown in figure 5.2b. A detailed drawing of this design is made in Solidworks and can be found in appendix B. When adding parts to a hydraulic system it is important that all air is removed from the system when it is filled with brake fluid, especially at the point where the pressure sensor measures the fluid pressure. When there is an air bubble right in front of the pressure sensor membrane, it will

measure the pressure of the compressed air bubble instead of the brake fluid pressure. Also, when there is air left in another place in the hydraulic system, the air will be compressed during braking and the moving force of the master piston will not or only partly translate to the slave pistons. To prevent these issues a pressure sensor with an 'in front' membrane is chosen. In most pressures sensor, the position of the membrane is more internal, what makes it harder to fill this area with pressure fluid. Also, the aluminum connection block is designed such that the pressure fluid can easily flow across the membrane without sudden gaps or edges. The pressure sensor that is used for this experiment is an ATM piezoresistive sensor. This sensor has a measuring range from 0-100 bar. According to Magura the maximum pressure of their brake systems is around 120 bar. Since a maximum pressure is not needed for this experiment, a maximum of 100 bar should be sufficient.

Working principle of a piezoresistive pressure sensor

Piezoresistive sensors use a membrane made of electrical resistive material. The electrical resistivity changes when the material is deformed [22]. This working principle is shown in figure 5.3.

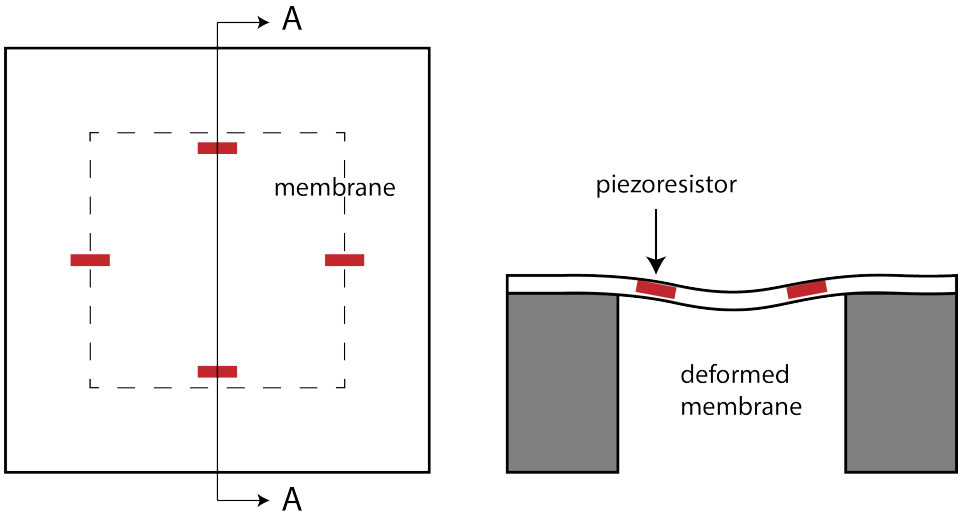

Figure 5.3: A schematic representation of the working principle of a piezoresistive pressure sensor [12].

Determination of the needed weight

In order to get realistic results it's important to determine how much friction force is needed during braking. For average braking (e.g. braking in front of a traffic light) we assume a braking time of 3s and an initial speed of 20 km/u. The friction force is defined as $F_{friction} = m_{bike} * a$, where $a = \Delta v/\Delta t$. Thus

$$F_{friction} = \frac{\Delta v}{\Delta t} * m, \tag{5.3}$$

where the speed v is in m/s, the time t is in s and the mass m is in kg. For the mass we take a mass of 85 kg including the bicycle. Calculating the braking force for these values it gives a force of $F_{friction} = 158N$. For each wheel the friction force is $157/2 = 79N$. The weight that is needed to imitate this friction force is the force divided by the gravitational acceleration: $79/9.81 = 8kg$. From this simple calculation it can be concluded that a weight of 8 kg is an appropriate weight to use for this experiment.

5.2. Measuring the static coefficient of friction

The static coefficient of friction is defined as $\mu_s = F_f/F_n$, where F_f is the friction force and F_n the normal force of the brake pads acting on the rim (figure 5.4). In the case of this experiment the friction force is equal to the gravity force (F_g) of the weight ($F_n = F_g$).

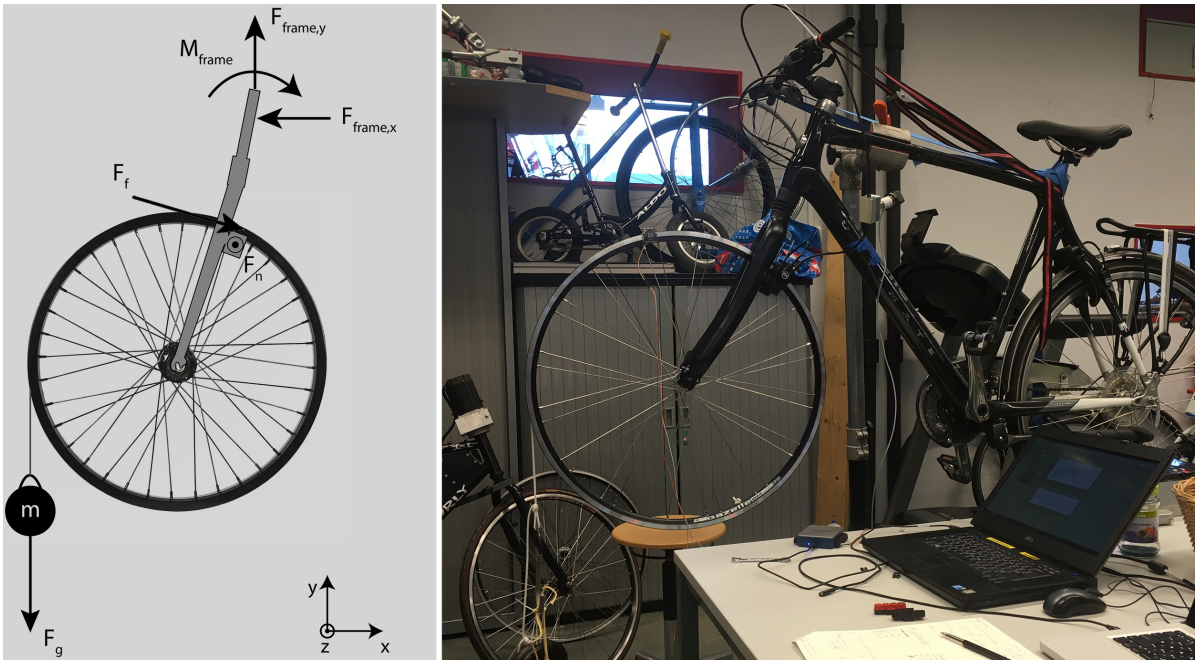

Figure 5.4: A free body diagram of the front wheel with a weight attached to the rim via a cord (left) and experimental setup (right).

The static coefficient of friction is measured by slowly decreasing the hydraulic pressure of the brake system until the wheel starts moving. In order to decrease the hydraulic pressure in small controllable steps, the other end of the brake lever is connected to the handle bar by a threaded end and three nuts (figure 5.5)a. The pressure sensor is connected to the brake system with the aluminum adapter. The data of the pressure sensor is sent to Labview via a Multifunction I/O device.

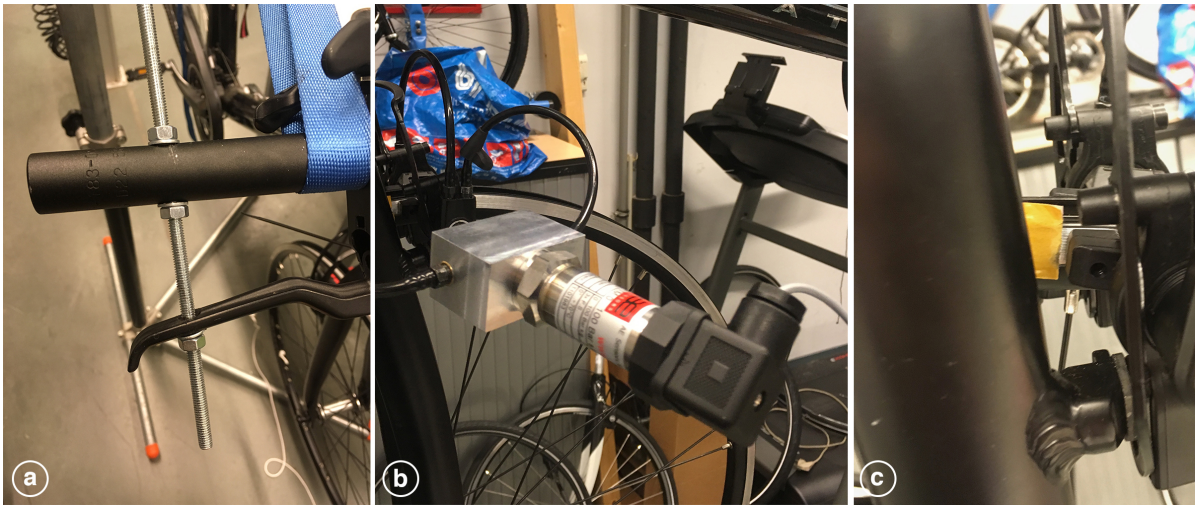

Figure 5.5: Brake lever connected to handle bar with threaded rod (a), fluid pressure sensor connected to the brake system and movement of the wheel is made visible with a little reference sticker attached to the rim (c).

Measuring procedure

First the nut on the threaded end is tightened to approximately 16 bar, to make sure that the wheel doesn't move when the weight is added. After adding the weight of 8 kg, the nut on the threaded end is slowly loosened with steps of approximately 1/3 rotation. Between each

step the movement of the rim is checked by looking closely at the rim on the location of the reference sticker (figure 5.5)c. At the start of the measurements it is made sure that there is no gap between the reference sticker and the brake pad. As soon as a small gap appears between the sticker and the brake pad, the measured pressure value is written down and the procedure is started over again.

Results

In this experiment four different brake pads are tested: Magura standard brake pads (black), Magura brake pads designed for aluminum rims (red), Elvedes brake pads and Trivio 3 components 950T brake pads. All these brake pads are made of rubber. For each brake pad type, the experiment is executed four times. The results are shown in table 5.1.

Table 5.1: Results of the static coefficient of friction coefficient measurements (in bar)

	Magura (zwart)	Magura (rood)	Compound	Elvedes
1	6.6 bar	7.3 bar	9.7 bar	8.8 bar
2	6.9 bar	7.3 bar	10.4 bar	9.1 bar
3	6.3 bar	6.5 bar	10.3 bar	9.1 bar
4	6.4 bar	6.5 bar	9.3 bar	8.0 bar
Average	**6.6 bar**	**6.9 bar**	**9.9 bar**	**8.8 bar**

The normal force of the brake pad on the rim can easily be calculated by multiplying the brake fluid pressure by the area of the piston surface:

$$F_n = p * A_{piston} = p * \pi * r^2. \tag{5.4}$$

According to Magura, the brake pads pistons have a diameter of 14 mm. Using this diameter, the actual coefficients of friction can be calculated (table 5.2.

Table 5.2: The calculated coefficients of friction based on the measured pressure values and the piston diameter.

	Magura (zwart)	Magura (rood)	Compound	Elvedes
1	0.77	0.70	0.52	0.58
2	0.74	0.70	0.49	0.56
3	0.80	0.78	0.50	0.56
4	0.80	0.78	0.55	0.64
Average	**0.78**	**0.74**	**0.52**	**0.59**

5.3. Measuring the dynamic coefficient of friction

As discussed earlier, the static coefficient of friction can be measured when the wheel starts rotating. At this point the wheel start to turn very slowly. It takes a few minutes before the gap between the reference sticker and the brake pad reaches a value of 1 cm. When loosening the nut on the threaded end, the speed of the wheel starts to increase slowly. At a certain point the wheel suddenly begins to accelerate until the weight hits the floor. This turning point will be used to measure the dynamic coefficient of friction. Figure 5.7 shows the sudden angular acceleration of the front wheel.

Measuring the angular velocity

To measure the angular velocity of the wheel a CRS03 angular rate sensor is used. This sensor is mounted on the rim with double sided tape and measures the angular speed in degrees/s. This sensor is connected together with the pressure sensor to the Multifunction I/O device to synchronize both sensor outputs precisely. The working principle of an angular rate sensor is comparable to the working of an accelerometer (explained in chapter 2) and is shown in figure 5.6. When the sensor starts rotating the mass moves towards the edge due to the centrifugal force acting on the mass. The relative motion of the mass with respect to the box will change the distance between the plates and therefore the capacitance of the

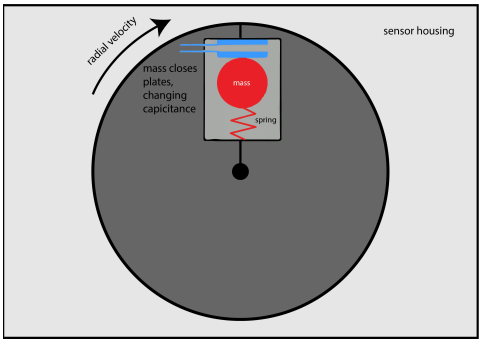

Figure 5.6: A schematic representation of the basic working principle of a angular rate sensor [10].

capacitor. The change in capacitance correspondents to the angular velocity of the sensor [10].

Strange pressure behavior

Figure 5.7 shows some strange behavior of the pressure in the hydraulic circuit of the brake system. When the nut on the threaded end is loosened step by step, the pressure first drops

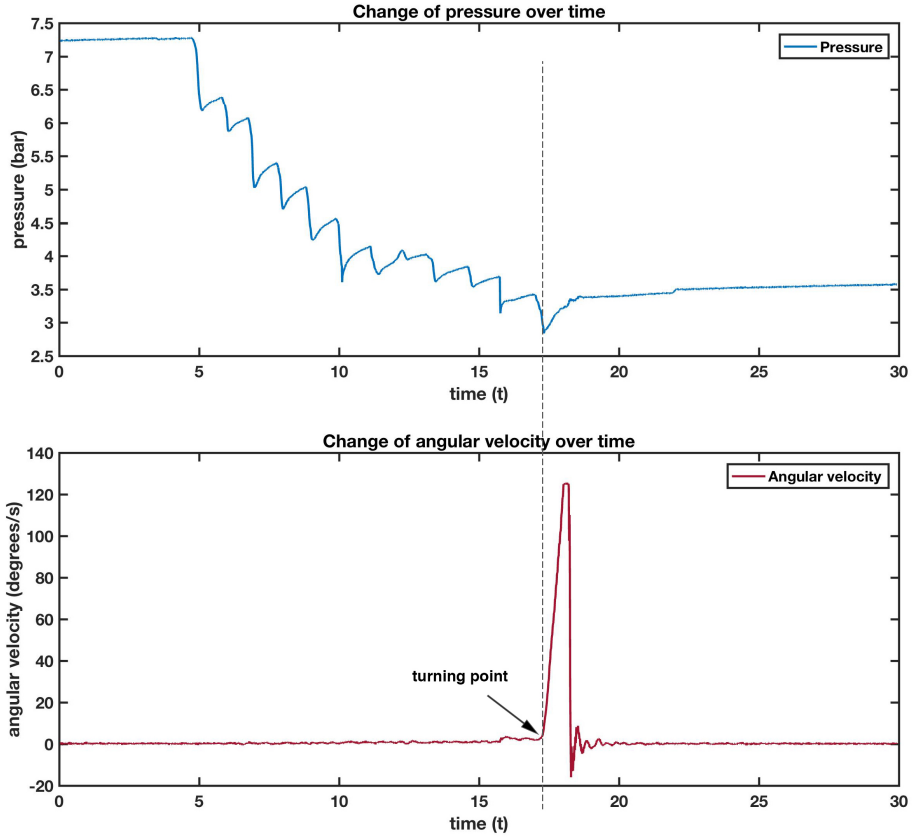

Figure 5.7: Brake fluid pressure is slowly decreased by loosening the nut on the threaded end in small steps (top) and at a certain point the wheel suddenly starts to accelerate (bottom).

instantly but starts to increase slowly again. This is probably due to the the friction between the brake pad pistons and the brake system housing. When the nut on the threaded end is loosened the piston of the brake lever reacts instantly causing a sudden drop in the brake pressure. The brake pad pistons on the other hand doesn't react instantly due to the high friction force of the pistons on the brake system housing. This friction force is bigger on

the slave pistons than on the master piston because of the gravitational force of the weight exerting on the rim. After the sudden drop in pressure the slave pistons slowly move back in the housing, causing the pressure to built up again.

Calculating the friction force

In contradiction to the static friction experiment, the friction force in this experiment is not equal to the gravity force of the weight. With the wheel accelerating there are two forces 'working against' the gravitational force of the weight. These forces are the inertia force of the weight itself and the inertia force of the wheel. The inertia force of the wheel is

$$F_{in,weight} = m_{weight} * a_{weight} = m_{weight} * \frac{d\omega}{dt} * r_{rim}, \tag{5.5}$$

where $d\omega/dt$ is the angular acceleration of the wheel in rad/s^2.

The inertia force of the wheel can be calculated by dividing the angular momentum of the rim and spokes by the radius of the moment:

$$F_{in,wheel} = \frac{I_{rim} * \frac{d\omega}{dt}}{r_{rim}} + \frac{I_{spokes} * \frac{d\omega}{dt}}{r_{spokes}}. \tag{5.6}$$

The inertia moment of the rim and spokes can be calculated with the formula

$$I = \frac{d\omega}{dt} * r^2 \tag{5.7}$$

Substituting this formula in previous formula gives

$$F_{in,wheel} = m_{rim} * r_{rim} * \frac{d\omega}{dt} + m_{spokes} * r_{spokes} * \frac{d\omega}{dt} \tag{5.8}$$

To calculate the friction force, the inertia forces of the weight and the wheel have to be subtracted from the the gravitational of the wheel:

$$F_{friction} = F_g - F_{in,weight} - F_{in,wheel}, \tag{5.9}$$

where $F_g = m_{weight} * g$.

Using the data from the pressure sensor and the contact area of the brake pad piston with the brake fluid, the normal force of the brake pads exerting on the rim can be calculated:

$$\mu_{kinetic} = \frac{F_{friction}}{F_{normal}} \tag{5.10}$$

Calculating the angular acceleration

The angular acceleration of the wheel can be determined by using the data of the angular rate sensor (figure 5.8). The angular acceleration can by calculated as following:

$$\frac{d\omega}{dt} = \frac{\Delta\omega}{\Delta t} \tag{5.11}$$

Also the average hydraulic pressure during the acceleration can be calculated by taking the average value of the pressure at the start of the acceleration and at the end of the acceleration. These data points can be read out by using Matlab.

The other needed values are listed below:
$m_{rim} = 0.63kg$, $m_{spokes} = 0.27kg$, $m_{weight} = 8kg$, $r_{rim} = 0.31m$, $r_{spokes} = 0.15m$, $r_{piston} = 0.007m$.
The diameter of the brake pad piston was given by Magura by email.

Results

For each brake pad type, the experiment is executed four times.

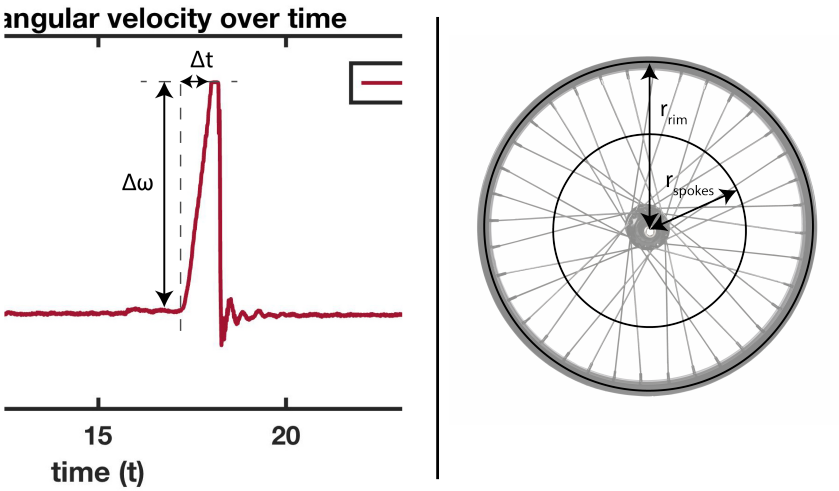

Figure 5.8: Using the data of the angular rate sensor to calculate the angular acceleration (left). The radius of the rim and spokes that is used to calculated to moment of inertia: $I = m * r^2$ (right).

Table 5.3: Magura original brake pads dynamic friction measurements.

	$\dot{\omega}(rad/s^2)$	$F_{in,total}$ (N)	$p_{average}$ (bar)	$F_f(N)$	$F_n(N)$	μ
1	1.29	3.5	3.1	75	49	1.5
2	1.33	3.6	3.2	75	49	1.5
3	1.22	3.2	3.2	75	49	1.5
4	1.60	4.4	3.2	74	49	1.5
Average						**1.5**

Table 5.4: Magura red brake pads dynamic friction measurements.

	$\dot{\omega}(rad/s^2)$	$F_{in,total}$ (N)	$p_{average}$ (bar)	$F_f(N)$	$F_n(N)$	μ
1	1.41	3.8	3.3	75	53	1.4
2	1.62	4.4	3.4	74	52	1.4
~~3~~	~~3.61~~	~~9.8~~	~~2.5~~	~~69~~	~~39~~	~~1.8~~
4	0.93	2.5	3.4	76	53	1.4
Average						**1.4**

Magura standard brake pads (black) results
The results for the original Magura brake pads are shown in table 5.3.

Magura brake pads designed for aluminum rims (red) results
The results for the Magura brake pads designed for aluminum rims are shown in table 5.4.

Elevedes brake pads results
The results for the original Magura brake pads are shown in table 5.5.

Elevedes brake pads results
The results for the Trivio 3 components 950T brake pads are shown in table 5.6.

Table 5.5: Elvedes brake pads dynamic friction measurements.

	$\dot{\omega}(rad/s^2)$	$F_{in,total}$ (N)	$p_{average}$ (bar)	$F_f(N)$	$F_n(N)$	μ
1	2.56	7.0	2.4	72	37	1.9
2	2.22	6.0	2.6	72	41	1.8
3	2.56	7.0	2.8	72	42	1.7
4	2.86	7.8	2.4	71	37	1.9
Average						**1.8**

Table 5.6: Trivio brake pads dynamic friction measurements.

	$\dot{\omega}(rad/s^2)$	$F_{in,total}$ (N)	$p_{average}$ (bar)	$F_f(N)$	$F_n(N)$	μ
1	1.15	3.1	3.5	75	54	1.4
2	2.69	7.3	3.0	72	47	1.5
3	3.40	9.3	2.8	69	43	1.6
4	2.50	6.8	3.0	72	47	1.5
Average						**1.5**

5.4. Discussion and Conclusion

An overview of the measured coefficients of friction of the different brake pads are shown in table 5.7. Also, the loudness of the noise is measured with a loudness meter. The frequencies are extracted from the recorded audio files. The results are added to the table.

Table 5.7: An overview of the measured coefficients of friction of the different brake pads.

	μ_s	μ_d	μ_d - μ_s	f (Hz)	Loudness (dB)
Magura black	0.78	1.5	0.72	1085	87
Magura red	0.74	1.4	0.68	1105	86
Trivio compound	0.52	1.5	0.98	1070	105
Elvedes	0.59	1.8	1.21	1067	100

While there are differences in friction coefficients, there are just minor differences in the squeal characteristics of the different brake pads. However, the relative high values of μ_d - μ_s for all brake pads point to stick-slip as the fundamental cause of the generated friction induced vibrations.

Discussion

Normally, the dynamic friction coefficient is lower than the static friction coefficient. However, the results of this experiment show the opposite. The dynamic friction coefficients are 2-3 time bigger than the static friction coefficient. This is probably due to the visco-elastic properties of rubber, since rubber is an elostomer. A study on dry friction between SBR (Styrol Butadieen Rubber) and smooth stainless steel shows similar results [1] (figure 5.9). It's hard to compare these results with results of the brake pad coefficients of friction, because the temperatures are different and the friction materials are slightly different. However, it confirms that the dynamic coefficient of friction can be 2-3 times bigger than the static coefficient of friction in the case of rubber-metal dry sliding contact. Also the order of magnitude of measured coefficient of frictions from both experiments resemble each other. This means that the measuring method and the calculations are correct.

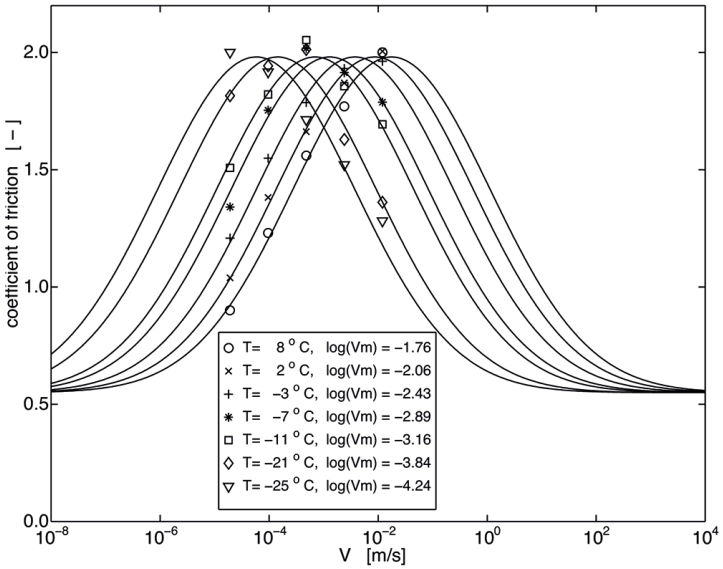

Figure 5.9: Results of a study on dry friction between SBR and smooth stainless steel [1].

6

Spoke tension

Spoke tension is probably an important factor when it comes to bicycle brake squeal, because the spoke tension is also directly related to the out-of-plane stiffness of the wheel. Most likely, this means that the spoke tension defines both the eigenfrequencies of the spokes and the eigenfrequency of the rim. If that is the case, spoke tension might also influence the squeal frequency. Furthermore, according to a study of Nakae et al. [15] (discussed in Chapter 1), spoke tension influences the squeal frequencies. However, in this study a bicycle with disc brakes is used instead of traditional rim brakes.

6.1. Experimental setup

The setup used for this experiment is shown in figure 6.1. A wheel truing stand is used to adjust and measure the spoke tension.

Figure 6.1: The setup for this experiment (a). A wheel truing stand is used to adjust and measure the spoke tension (b).

6.2. Working principle of a spoke tension meter and calibration

A spoke tension meter uses a torsion spring to clamp the spoke between three small cylinders (figure 6.2a). By clinching the tension meter, the lower cylinder in figure 6.2b cylinder is moving to the bottom. After attaching the tension meter to the spoke the tension is released. How far the meter moves back depends on the tension in the spoke. The more it moves back, the lower the tension. The value that is read from the tension meter has to be converted to a real measurement value using the conversion table (Appendix C) that comes with the tension meter.

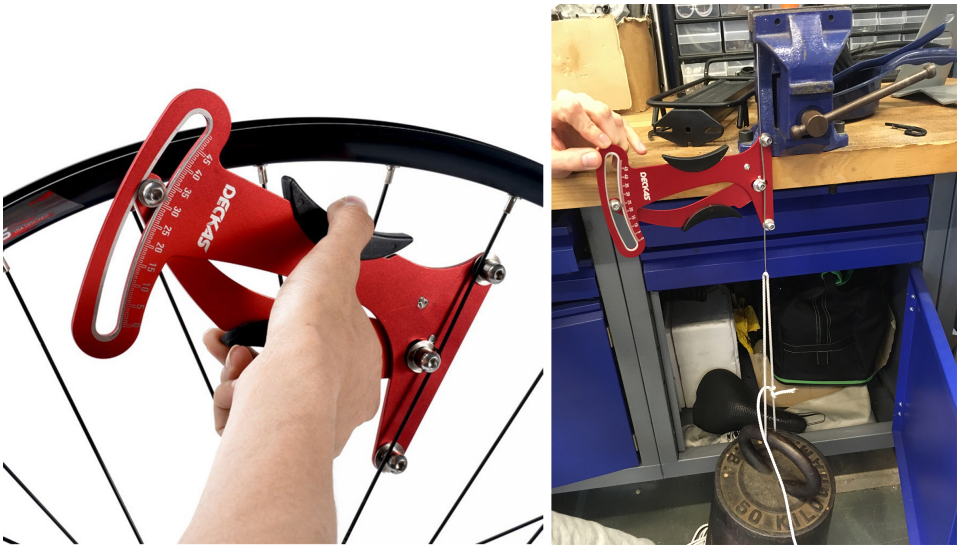

Figure 6.2: The working principle of a spoke tension meter.

The converted value has a unit of kgf (1kgf = 9.8N). For calibration a weight of 50 kg is a attached to the bottom of the spoke by a wire. The top of the spoke is fixed into a vise. According to the conversion table a weight of 50 kg should correspondent with a number of 25 on the spoke tension meter. The stiffness of the radial spring was adjusted until the spoke tension meter measured 25 with a spoke tension of 50 kgf.

6.3. Measurement procedure

The spoke tension was increased and decreased by steps of half rotations per spoke nipple. After each step, the tension of six labeled spokes was measured with the spoke tension meter. When the desired spoke tension was reached, the wheel was mounted in the bicycle and the treadmill was used to let the bicycle squeal.

6.4. Results

The conversion table that came with the spoke tension meter has only a certain range (Appendix C). The lowest measured value is 25 and the highest 34 for spokes with a diameter of 2.0 mm. Spoke tension values out of this range are probably never used. A value of 25 correspondents to 49 kgf and 34 correspondents to 160 kgf. Within this range, the frequencies of four different spoke tension values were measured. Also, the frequency of one very low spoke tension value is measured. When the spoke tension is very low, the spokes don't contribute to the out of plane stiffness of the wheel. This will probably influences the brake squeal frequency or behavior. The squeal frequencies are extracted from the recorded audio files using Adobe Audition.

The results are shown in table 6.1.

Table 6.1: The measured spoke tensions with their corresponding squeal frequencies.

Measured value	Spoke tension (Kgf)	Squeal frequency (Hz)
14	?	1096
25	49	1092
28	70	1097
31	100	1092
34	160	1088

The measured value is coming from the spoke tension meter and has no unit. The spoke tension in Kgf comes from the conversion table (Appendix C). For the measured value of 14, there is no spoke tension value available, since it is out of range of the conversion table.

6.5. Discussion and Conclusion

From the results it can be seen that the spoke tension barely influences the squeal frequency of the bicycle during braking. Also the squeal propensity was roughly the same for all spoke tensions. From these results can also be concluded that the out-of-plane stiffness of the wheel doesn't influence the squeal frequency and propensity, because a higher spoke tension means also a higher out of plane stiffness of the wheel.

7

Discussion

This chapter contains a general discussion of this graduation project in its entirety, since more in depth discussions of the individual experiments are already included in chapter 2-6.

In Chapter 3 all 17 potential squeal parameter were shown in a diagram. Only 5 of the 17 parameter were studied in this graduation project. This means that this project is only a starting point into the world of bicycle brake squeal. For example, rain and dirt are also known as an important factors when it comes to bicycle brake squeal propensity. Furthermore, in most experiments of this graduation project, a treadmill is used to let the bicycle squeal. A treadmill allows to brake continuously with more or less constant brake force. In reality, braking happens with a varying brake pressure and wheel speed. However, this graduation project has given more insight in the fundamental cause of bicycle brake squeal and showed which parameters influence brake squeal and propensity.

8

Conclusion

This chapter contains a general conclusion of this graduation project in its entirety, since more in depth conclusions of the individual experiments are already included in chapter 2-6.

The most important conclusions are listed below:

1. First of all can be concluded that stick-slip is most probably the fundamental cause of bicycle brake squeal. The measurements with the accelerometer and laser vibrometer (Chapter 1) showed that the brake pads are vibrating in the rotating direction of the rim. Also, the brake pad friction coefficient experiment (Chapter 5) showed big differences between the static and dynamic friction coefficients of the brake pads. These results strongly point to stick-slip is the fundamental cause of bicycle brake squeal.

2. The stiffness of the front fork appeared to be an important factor. The measurements with the accelerometer showed that the front fork is vibrating in the same frequency as the brake pads. This means that the vibration of the brake pad is transmitted to the front fork. Furthermore, changing the fork also changes the squeal frequency and the squeal propensity (Chapter 4).

3. The laser vibrometer results showed that the vibration mode of the front fork is a combination of out-of-plane vibration and torsional vibration. The out-of-plane vibration of the front fork wall, indicates that the fork is functioning as a resonance box, amplifying the vibrations coming from the brake pads. After adding a brake booster, the squeal was gone. Also, the torsional vibrations were gone. Apparently, the torsional stiffness of the front fork is an important factor when it comes to bicycle brake squeal.

4. Changing the front fork is the only way to change the squeal frequency. Other components as rim, spokes, brake pads and tire don't influence the squeal frequency.

5. From the spoke tension experiment in Chapter 6 was concluded that the spoke tension doesn't influence the squeal frequency and propensity. Also, the out-of-plane stiffness of the rim doesn't influence the squeal frequency and propensity, since the spoke tension and the out-of-plane stiffness of the rim are strongly correlated.

9

Recommendations

As discussed earlier, the stiffness of the front fork determines whether a bicycle is going to squeal. A big advantage of the front fork stiffness is that it doesn't change over time. Other parameters like friction coefficient of the brake pads, spoke tension and weather conditions are changing over time. The front fork has to be designed such that brake squeal can never occur, independently of all the other parameters. Therefore, it is recommended to focus on the fork in the next study on bicycle brake squeal.

Also, during the experiments, the masses of the front fork, the front hub, the rim and tire seemed to play an important factor in squeal propensity.

Finally, adding damping material to the inside of the front fork will probably decrease the loudness of the brake squeal, since the front fork is most likely acting like a resonance box, amplifying the vibration coming from the brake pads.

A

```
A = importdata('metingen/meting9_spaak.csv');

% creating a time vector that correspondents to the data
D = size(A);
Nsamps = D(1,1);
fsamp = 20000;
Tsamp = 1/fsamp;
t = (0:Nsamps-1)*Tsamp;

x = A(:,1);     % acceleration data in x-direction
y = A(:,2);     % acceleration data in y-direction
z = A(:,3);     % acceleration data in z-direction

% plotting all data
plot(t,x,t,y,t,z)
legend('x','y','z')
%% plot a small portion (400 measuring points) in the middle of the data
p1 = 0.5*Nsamps;
p2 = p1+400;

x1 = x(p1:p2);
y1 = y(p1:p2);
z1 = z(p1:p2);
t1 = t(p1:p2);

% normalize data
x2 = x1-mean(x1);
y2 = y1-mean(y1);
z2 = z1-mean(z1);

plot(t1,x2,t1,y2,t1,z2)
legend('x','y','z')
xlabel('Time (s)')
ylabel('Acceleration (g)')
title('Plot of the acceleration of the front fork vs time')

%% FFT accelerometer
p1 = Nsamps/2;
p2 = p1+10000;

Fs = 20000;

x1 = x(p1:p2);
y1 = y(p1:p2);
z1 = z(p1:p2);
t1 = t(p1:p2);

nfft = length(x1);
nfft2 = 2^nextpow2(nfft);
ff = fft(x1);
fff = ff(1:nfft/2);
xfft = Fs*(0:nfft/2-1)/nfft;
plot(xfft(5:end),abs(fff(5:end)))
```

B

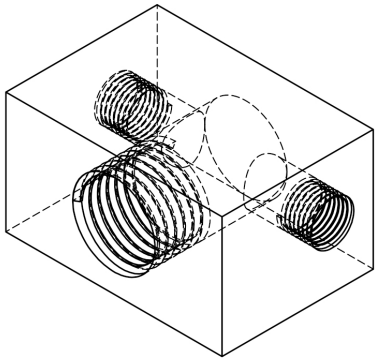

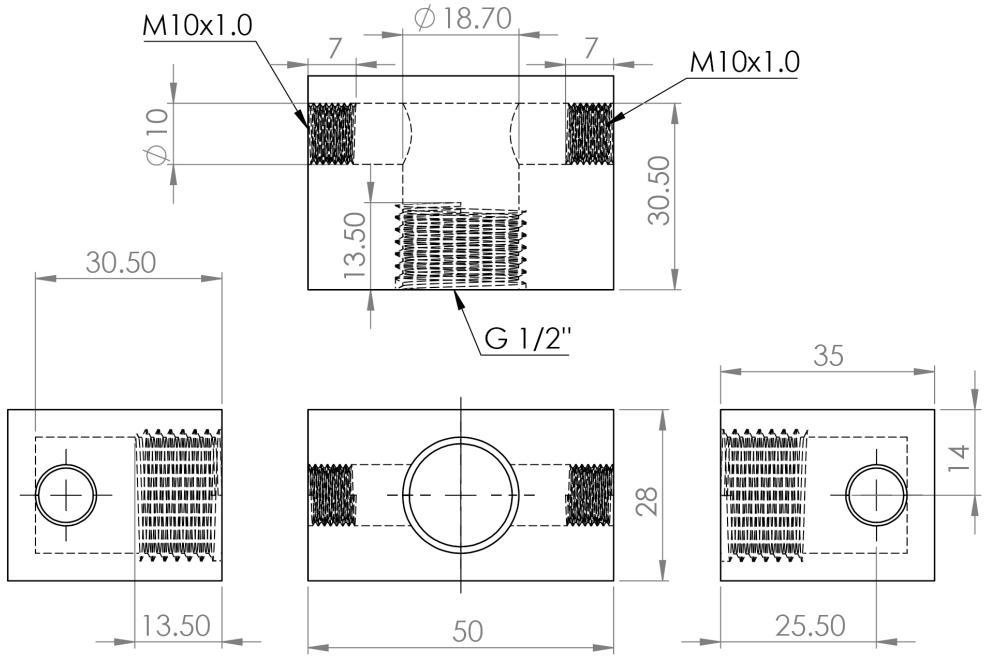

G 1/2": thread pitch = 1.814 mm, major diameter = 20.955 mm , minor diameter = 18.631 mm, gauge length: 8.2 mm

UNLESS OTHERWISE SPECIFIED: DIMENSIONS ARE IN MILLIMETERS SURFACE FINISH: TOLERANCES: LINEAR: ANGULAR:	FINISH:	DEBURR AND BREAK SHARP EDGES	DO NOT SCALE DRAWING	REVISION	
	NAME	SIGNATURE	DATE	TITLE:	
DRAWN					
CHK'D					
APPV'D					
MFG					
Q.A				DWG NO.	A4
				aluminium blokje	
				SCALE:1:1	SHEET 1 OF 1
			WEIGHT:		

C

Conventible Table

Spoke Tension [kgf] (1kgf=9.8Nm=2.2lb)

SPOKE SIZE	Butted Spokes						Bladed Spokes											
Measured Reading	2.3	2.0	1.8	1.7	1.6	1.5	3.0*1.1	3.2*1.1	2.1*0.95	4.5*1.0	2.0*0.9	1.7*0.9	2.8*1.3	2.2*0.9	2.3*0.9	3.3*1.1	2.3*1.2	2.25*1.2
6																		
7																		
8																		
9																		
10																		
11																		
12									48		47			46	46			
13									52		52	48		50	50			
14									56		57	53		55	57			
15							47		61		62	58		60	64			
16							51	46	66	48	68	64		65	71	47		
17							57	51	71	55	74	71		71	78	51	49	
18						46	63	56	78	62	81	79		77	85	57	56	47
19					45	51	69	61	86	70	88	87		85	92	64	64	53
20				46	50	57	76	68	98	78	95	95	49	94	99	71	72	62
21				50	55	63	85	76	110	86	105	103	56	105	110	78	80	70
22			48	55	60	69	96	85	122	96	120	115	63	118	128	88	88	78
23			53	60	65	76	109	96	141	111	135	132	71	133	144	99	96	86
24			59	68	73	85	122	107	162	127	155	150	80	150	160	111	111	94
25		49	65	79	83	95	138	122		145		170	90	170		127	129	109
26		56	75	90	94	108	154	142		163			105			147	147	127
27		63	85	102	105	122		162					120			170	167	145
28		70	96	114	119	136							140					165
29		80	110	131	138	156							160					
30	42	90	125	150	157													
31	50	100	141	169														
32	57	120	160															
33	64	140																
34	77	160																
35	95																	
36	110																	
37	134																	
38	157																	
39																		
40-45																		

Bibliography

[1] J. P. Meijaard A. R. Savkoor. Application of bifurcation theory to the identification of the constitutive relations for sliding friction. In *IUTAM Symposium on Nonlinearity and Stochastic Structural Dynamics*, pages 233–248, 2001.

[2] A. Akay. Acoustics of friction. *The Journal of the Acoustical Society of America*, 111(4): 1525–1548, 2002.

[3] T. R. Bedding. Introduction to interferometry. 2006.

[4] A. Le Bot, E. Bou-Chakra, and G. Michon. Dissipation of vibration in rough contact. *Tribology Letters*, 41(1):47–53, Jan 2011.

[5] N. M. Ghazaly and M. El-Sharkawy nad I. Ahmed. A review of automotive brake squeal mechanisms. *Journal of Mechanical Design and Vibration*, 1(1):5–9, 2013.

[6] Jasna Glisovic, R RadonjiA, and Danijela MiloradoviA. Experimental method for analyzing friction phenomenon related to drum brake squeal. *Tribology in Industry*, 32:28–35, 12 2010.

[7] M. Graf and G.P. Ostermeyer. Friction-induced vibration and dynamic friction laws: Instability at positive friction–velocity-characteristic. *Tribology International*, 92:255 – 258, 2015.

[8] N. Hoffmann, M. Fischer, R. Allgaier, and L. Gaul. A minimal model for studying properties of the mode-coupling type instability in friction induced oscillations. *Mechanics Research Communications*, 29(4):197 – 205, 2002.

[9] R. Ibrahim. Friction induced vibratoin. In S. Braun, editor, *Encyclopedia of Vibration*, pages 589 – 596. Elsevier, Oxford, 2001.

[10] D. Krakauer J. Geen. *Angular-Rate-Sensing Gyroscope*, 2003. URL `https://www.analog.com/en/analog-dialogue/articles/imems-angular-rate-sensing-gyroscope.html`.

[11] H. Keitzel and N. Hoffmann. Influence of the contact model on the onset of sprag-slip. *PAMM*, 6(1):311–312, 2006.

[12] Ali Kubba, Ahmed Hasson, Ammar Kubba, and Gregory Hall. A micro-capacitive pressure sensor design and modelling. *Journal of Sensors and Sensor Systems*, 5:95–112, 03 2016.

[13] R. Lima and R. Sampaio. Parametric analysis of the statistical model of the stick-slip process. *Journal of Sound and Vibration*, 397:141 – 151, 2017.

[14] T. Nakae, T. Ryu, and A. Sueoka. Nonlinear analysis of chatter phenomena generated in a bicycle disc brake. *Transition of the Japan society of mechanical engineers series C*, 77(774):493–504, 2011.

[15] T. Nakae, T. Ryu, A. Sueoka, Y. Nakano, and T. Inoue. Squeal and chatter phenomena generated in a mountain bike disc brake. *Journal of Sound and Vibration*, 330(10):2138 – 2149, 2011. Dynamics of Vibro-Impact Systems.

[16] T. Nakae, A. Sueoka, and T. Ryu. Analytical investigation on squeal phenomena generated in bicycle disc brakes. *Transition of the Japan society of mechanical engineers series C*, 77(774):481–492, 2011.

[17] S. Oberst and J.C.S. Lai. Chaos in brake squeal noise. *Journal of Sound and Vibration*, 330(5):955 – 975, 2011.

[18] H. Olsson, K.J. Åström, C. Canudas de Wit, M. Gäfvert, and P. Lischinsky. Friction models and friction compensation. *European Journal of Control*, 4(3):176 – 195, 1998.

[19] Polytec. *Basic principles of vibrometry*, 2019. URL `https://www.polytec.com/us/vibrometry/basic-principles-of-vibrometry/`.

[20] R. Redfield. *Brake Induced Vibration in Mountain Bikes (P112)*. Paris, 2008.

[21] R. Redfield. Bike braking vibration modelling and measurement. *Procedia Engineering*, 72:471 – 476, 2014. The Engineering of Sport 10.

[22] Paul P.L. Regtien. 4 - resistive sensors. In Paul P.L. Regtien, editor, *Sensors for Mechatronics*, pages 57 – 100. Elsevier, Oxford, 2012.

[23] S.K. Rhee, P.H.S. Tsang, and Y.S. Wang. Friction-induced noise and vibration of disc brakes. *Wear*, 133(1):39 – 45, 1989.

[24] S.C. Tiwari. Doppler effect and frequency-shift in optics. 2008.

[25] M. Triches Jr, S. N. Y. Gerges, and R. Jordan. Reduction of squeal noise from disc brake systems using constrained layer damping. *Journal of the Brazilian Society of Mechanical Sciences and Engineering*, 26:340–348, 2004.

[26] V. van Geffen. A study of friction models and friction compensation. Master's thesis, Technische Universiteit Eindhoven, December 2009.

[27] D.W. Wang, J.L. Mo, Q. Zhang, J. Zhao, H. Ouyang, and Z.R. Zhou. The effect of the grooved elastic damping component in reducing friction-induced vibration. *Tribology International*, 110:264 – 277, 2017.

[28] C. Woodford. *Accelerometers*, 2018. URL `https://www.explainthatstuff.com/accelerometers.html`.

[29] M. Yokoi and M. Nakai. A fundamental study on frictional noise : 1st report, the generating mechanism of rubbing noise and squeal noise. *Bulletin of JSME*, 22(173):1665–1671, 1979.